Progression of Meiosis Is Coordinated by the Level and Location of MAPK Activation Via OGR-2 in *Caenorhabditis elegans*

Hanna Achache,* Lévana Laurent,* Yaël Hecker-Mimoun,* Hasan Ishtayeh,* Yisrael Rappaport,* Eitan Kroizer,* Monica P. Colaiácovo,† and Yonatan B. Tzur*,[1]

*Department of Genetics, Institute of Life Sciences, Hebrew University, Givat-Ram, Jerusalem 91904, Israel and †Department of Genetics, Harvard Medical School, Boston, Massachusetts 02115

ORCID ID: 0000-0002-7715-6113 (Y.B.T.)

ABSTRACT During meiosis, a series of evolutionarily conserved events allow for reductional chromosome division, which is required for sexual reproduction. Although individual meiotic processes have been extensively studied, we currently know far less about how meiosis is regulated and coordinated. In the *Caenorhabditis elegans* gonad, mitogen-activated protein kinase (MAPK) signaling drives oogenesis while undergoing spatial activation and deactivation waves. However, it is currently unclear how MAPK activation is governed and how it facilitates the progression of oogenesis. Here, we show that the *oocyte and germline-related 2* (*ogr-2*) gene affects proper progression of oogenesis. Complete deletion of *ogr-2* results in delayed meiotic entry and late spatial onset of double-strand break repair. Elevated levels of apoptosis are observed in this mutant, independent of the meiotic canonical checkpoints; however, they are dependent on the MAPK terminal member MPK-1/ERK. MPK-1 activation is elevated in diplotene in *ogr-2* mutants and its aberrant spatial activation correlates with stages where meiotic progression defects are evident. Deletion of *ogr-2* significantly reduces the expression of *lip-1*, a phosphatase reported to repress MPK-1, which is consistent with OGR-2 localization at chromatin in germ cells. We suggest that OGR-2 modulates the expression of *lip-1* to promote the timely progression of meiosis through MPK-1 spatial deactivation.

KEYWORDS fertility; meiosis; oogenesis

MEIOSIS is a specialized, coordinated program of cell division where one cycle of chromosome duplication is followed by two consecutive rounds of segregation. This process reduces the chromosome number by half, thereby generating haploid gametes from diploid cells. This reduction is achieved through unique and highly coordinated chromosomal interactions where homologous chromosomes pair, align, and form physical connections prior to the first division [reviewed in Jasin and Rothstein (2013), Lui and Colaiacovo (2013), Mézard *et al.* (2015), and Gray and Cohen (2016)]. A challenging question in the study of meiosis is: how are these intricate interactions controlled and phased?

doi: https://doi.org/10.1534/genetics.119.302080
Manuscript received December 7, 2018; accepted for publication March 7, 2019; published Early Online March 12, 2019.
Supplemental material available at https://doi.org/10.25386/genetics.7825712.
[1]Corresponding author: Department of Genetics, Institute of Life Sciences, Hebrew University, Givat-Ram, Jerusalem 91904, Israel. E-mail: tzur@mail.huji.ac.il

The nematode *Caenorhabditis elegans* is an excellent model organism that is especially suited for investigating how meiosis is governed and orchestrated. In the hermaphrodite gonad arm, nuclei are arranged in a well-defined spatial temporal order from the stem cell niche to the fertilized embryo, enabling cytological observations of all meiotic stages at the same time and in the same organ. The distal region of the *C. elegans* gonad, termed the mitotic zone or the proliferative zone, contains proliferating germ cell nuclei (Kimble and White 1981). This proliferation is essential for maintaining the progenitor pool that repeatedly produces meiocytes. As cells move proximally, they enter meiosis in the leptotene/zygotene (LZ or transition) zone, where recognition and pairing of homologous chromosomes are initiated. At this time, double-strand break (DSB) formation commences, catalyzed by SPO-11, a highly conserved topoisomerase-like endonuclease (Keeney *et al.* 1997; Dernburg *et al.* 1998), and repair begins via homologous recombination

(Dernburg *et al.* 1998). As nuclei enter the pachytene stage, a tripartite proteinaceous scaffold, known as the synaptonemal complex (SC), holds pairs of homologous chromosomes together (MacQueen *et al.* 2002; Schild-Prüfert *et al.* 2011). Throughout this stage, most meiotic crossover (CO) events mature within the context of fully synapsed chromosomes. During diplotene, the SC starts to disassemble and homologs remain attached mostly by a single chiasma, the cytologically detectable connection, resulting from a crossing-over event that occurred in each of the homologous chromosomes. At the diakinesis stage, six discrete bivalents (pairs of homologs) can be detected in mature oocytes. Timely progression of each stage during meiosis is a prerequisite for the formation of functional euploid gametes [reviewed in Lui and Colaiacovo (2013) and Hillers *et al.* (2017)]. However, our current understanding of the regulatory mechanisms that dictate meiotic progression is highly limited and further research is required.

Mitogen-activated protein kinase (MAPK) signaling is a master regulator of key meiotic events in *C. elegans* (Gumienny *et al.* 1999; Yin *et al.* 2016). This pathway includes the signaling molecules LET-60 (Ras), LIN-45 (Raf), and MEK-2 (Mek), which relay extracellular signals that result in phosphorylation and activation of its terminal member MPK-1 (Erk) (Chen *et al.* 2001). Active MPK-1 phosphorylates substrates that control and coordinate multiple essential aspects of *C. elegans* germline development [reviewed in Arur (2017)]. MPK-1 activation is temporally regulated; it is activated in pachytene, where its signal regulates pachytene progression and exit (Lee *et al.* 2007b). Indeed, mutations in any of the core genes in the MAPK signaling pathway—namely, *let-60*, *lin-45*, *mek-2*, or *mpk-1*—result in a pachytene-arrest phenotype, *i.e.*, the failure of germ cells to successfully progress from pachytene into diplotene (Church *et al.* 1995; Gumienny *et al.* 1999). After pachytene exit, MPK-1 is rapidly inactivated. This inactivation was previously attributed to LIP-1, a nematode homolog of the vertebrate's MAPK phosphatases (Hajnal and Berset 2002; Rutkowski *et al.* 2011). As the oocytes approach the spermatheca, the secreted sperm signal, MSP, reactivates MPK-1, which consequently induces oocyte maturation and allows meiosis to progress (Miller *et al.* 2001; Kosinski *et al.* 2005). When either synapsis or DSB repair (DSBR) is not completed, owing to various environmental or genetic causes, most of the affected meiocytes are eliminated by germ cell apoptosis (Gartner *et al.* 2000, 2008). However, this quality control mechanism is prevented if MAPK signaling is blocked and, conversely, it occurs at excessive levels in null *lip-1* mutants, where MPK-1 activity was suggested to be increased (Hajnal and Berset 2002; Lee *et al.* 2006; Rutkowski *et al.* 2011). MPK-1 also has a nonessential function in promoting the proliferative germ cell fate. Null *mpk-1* mutants have a small germline, which can be explained by reduced germline stem cell proliferation (Lee *et al.* 2007a,b; Narbonne *et al.* 2017). MPK-1 controls and coordinates other essential aspects of cell biology during oogenesis, including cellular organization, SC disassembly, oocyte organization, and differentiation, as well as oocyte maturation and ovulation (Lee *et al.* 2007b; Nadarajan *et al.* 2016). Therefore, MAPK signaling acts at nearly all stages of oogenesis; it has been suggested to be a major contributor to meiotic coordination (Arur 2017). Even though the different roles of MPK-1 in meiosis have been extensively studied, our knowledge of the underlying mechanisms controlling its spatial activation, allowing meiotic progression, remains incomplete.

Here, we describe the meiotic roles of the previously uncharacterized SPK [SET (Su(var)3-9, Enhancer-of-zeste and Trithorax) and PHD (plant homeodomain) domain-containing proteins, and protein kinases] domain-containing OGR-2 protein. Loss of *ogr-2* affects several processes, ranging from entering into meiosis to mature oocytes' fates, as well as the correct formation of bivalent structures. Deletion of *ogr-2* leads to high levels of germ cell apoptosis through a noncanonical MPK-1-dependent pathway. In agreement with these results, we found that *ogr-2* negatively influences the spatial activation of MPK-1 in the gonad. Importantly, we show that *ogr-2* and *lip-1* mutants exhibit similar, but nonadditive, defects in germline development and in the regions of MPK-1 activation, indicating that they act through the same genetic pathway. OGR-2 is localized to the chromatin of germ cells in foci and patches, which can explain the *ogr-2* requirement for normal levels of *lip-1* mRNA. These findings suggest that *ogr-2* may act via *lip-1* to control the level and location of MAPK signaling activation, thereby coordinating the timely progression of key meiotic processes.

Materials and Methods

Strains and alleles

All strains were cultured under standard conditions at 20° unless specified otherwise (Brenner 1974). The N2 Bristol strain was utilized as the wild-type background. Worms were grown on NGM plates with *Escherichia coli* OP50 (Brenner 1974). Unless otherwise stated, all experiments were conducted using adult hermaphrodites 20–24-hr post-L4 stage. The following mutations and chromosome rearrangements were used: LGI: *hus-1(op241)*, *cep-1(gk138)*, LGII: *meIs8* [*pie-1p*::*GFP*::*cosa-1* + *unc-119*(+)] II, LGIII: *mpk-1(ga111)*, LGIV: *lip-1(zh15)*, and LGV: *syp-1(me17)* V/*nT1 [unc-?(n754) let-? qIs50]* (IV;V). The following strains have been previously described: UV7: *unc-119(ed3)* III; *jfIs2[piepromoter::GFP::zhp-3]* (Bhalla *et al.* 2008), CV64: *rjEx02[-Ppie-1::GFP::lab-1::HA; unc-119(+)]* (de Carv alho *et al.* 2008), and RW10226: *stIs10226[his-72p::HIS-24::mCherry::let-858 39 UTR + unc-119(+)]* (Murray *et al.* 2012).

The YBT5: *ogr-2(huj1) II*, YBT38: *ogr-2(huj18) II*, and YBT44: *ogr-2*(*huj20*[*ogr-2*::*3XFLAG*]) II strains were generated by clustered regularly interspaced short palindromic repeat (CRISPR)-Cas9 engineering (see below). Homozygous *ogr-2(huj1)* worms were outcrossed five times with the N2 wild-type strain. Unless otherwise stated, all experiments and

downstream crosses reported here were carried out using the outcrossed strain.

Generation of ogr-2-engineered strains by CRISPR-Cas9 genome editing

To generate the *ogr-2(huj1)* deletion, we used the procedure described in Friedland *et al.* (2013), but with several modifications. We used the following plasmids: *pU6*::*unc-119* sgRNA (single-guide RNA) (Friedland *et al.* 2013) and *peft-3*::cas9-SV40_NLS::tbb-2 3UTR (Friedland *et al.* 2013), together with the co-injection markers pCFJ90 (*pmyo-2*::*mCherry*::*unc-54utr*) (plasmid # 19327; Addgene) and pCFJ104 (*pmyo-3*::*mCherry*::*unc-54*) (plasmid # 19328; Addgene), which were a kind gift from Erik Jorgensen. We generated four new sgRNA plasmids by site-directed mutagenesis PCR (Weiner *et al.* 1994) with the vector *pU6*::*unc-119* sgRNA to replace *unc-119* with the sgRNA of interest [see below and Friedland *et al.* (2013)]. We designed *ogr-2* sgRNAs to target two DNA sites before the ATG codon of *ogr-2* ORF and two sites after the stop codon. The sequences of the sgRNAs were as follows:

ogr-2-sgRNA-1: 5′-ACC GCA AAC TCA CGA GAT GC-3′.
ogr-2-sgRNA-2: 5′-AAA ATA TAT TGT TTT CTT TC-3′.
ogr-2-sgRNA-3: 5′-ACG ATA CTT GAC AGC ACT GG-3′.
ogr-2-sgRNA-4: 5′-GAA ATT TTA AAA AAC TCA AG-3′.

Transgenic worms were created via microinjection of a mixture of DNA plasmids into the syncytial gonad of young adult N2 worms as described previously (Friedland *et al.* 2013; Tzur *et al.* 2013). The injection mix contained the following plasmids: four *ogr-2* sgRNAs at 50 ng/μl each, *peft-3*::cas9-SV40_NLS::*tbb-2* 3UTR at 100 ng/μl, pCFJ90 at 5 ng/μl, and pCF104 at 100 ng/μl. Transformants were selected by isolating marker-positive (mCherry+) worms.

A second *ogr-2* deletion strain, YBT38, was generated by CRISPR-Cas9/crRNA-tracrRNA ribonucleprotein (RNP) injection using the protocol described in Paix *et al.* (2015). Two *ogr-2*-gRNAs (analogous to *ogr-2*-sgRNA-2 and 3) were used.

We tagged the *ogr-2* gene by inserting 3XFLAG before the stop codon using CRISPR-Cas9/RNP complexes containing an *ogr-2*-FLAG-sgRNA and an ssODN repair template that included a 66-nt insert coding for a 3XFLAG tag: Ogr-2-flag-sgRNA: 5′-ATATCTTCCGACATGTATTA-3′ and 3XFLAG ssODN sequence: 5′-GACTACAAAGACCATGACGGTGATTATAAAGATCATGATATCGATTACAAGGATGACGATGACAAG-3′.

Fecundity assays

To determine the fecundity of the *ogr-2* mutants, at least 19 individual L4 worms were placed on seeded NGM plates, transferred to new plates every 24 hr, and their embryos and hatched progeny were counted during a 3-day period.

To determinie the *mpk-1(ga111)* effects on brood size, mutant lines were maintained at 15° before initiating the assays, being isolated at the L4 stage, and were maintained at 25° throughout the analyses.

Cytological analysis and immunostaining

DAPI and immunostaining of dissected gonads were carried out as described in Colaiácovo *et al.* (2003) and Saito *et al.* (2009). Worms were permeabilized on Superfrost+ slides for 2 min with methanol at −20° and fixed for 30 min in 4% paraformaldehyde/phosphate-buffered saline (PBS). Staining with DAPI was carried out for 10 min at 500 ng/ml, followed by destaining in PBS containing 0.1% Tween 20 (PBST); then, the slides were mounted with Vectashield antifading medium (Vector Laboratories, Burlingame, CA). Primary antibodies were used at the following dilutions: rabbit α-LAB-1 (1:200) (de Carvalho *et al.* 2008), rabbit α-RAD-51 (1:10,000, SDIX), mouse α-MAPK-YT (1:500, M8159; Sigma [Sigma Chemical], St. Louis, MO), rabbit α-SYP-2 (1:200, a kind gift from S. Smolikove), rabbit α-pH3 (D5692, 1:1000; Sigma), mouse anti-FLAG M2 (F1804, 1:500; Sigma), rabbit anti-HIM-8 (1:200; Novus Biological), and guinea pig α-HTP-3 (1:200) (Goodyer *et al.* 2008). The secondary antibodies used were Cy2-goat anti-rabbit, Cy3-goat anti-rabbit, Cy3-goat anti-mouse, and Cy2-donkey anti-guinea pig (all used at 1:500 dilution; Jackson ImmunoResearch Laboratories, West Grove, PA).

Imaging and microscopy

For GFP::ZHP3, α-pH3, mouse anti-FLAG M2, double-phosphorylated MPK-1 (dpMPK-1) immunostaining, and DIC visualization, images were acquired using the Olympus IX83 fluorescence microscope system (Olympus). Optical Z-sections were collected at 0.30/0.60-μm increments with a Hamamatsu Orca Flash 4.0 v3 and CellSens Dimension imaging software (Olympus). Pictures were deconvolved using AutoQuant X3 (Media Cybernetics).

For bivalent analysis and LAB-1, SYP-2, HTP-3, HIM-8, and RAD-51 immunostaining, Z-stack three-dimensional (3D) images were taken at 0.3-μm increments using an Olympus FV1000 Inverted Confocal IX81 microscope and FV10-ASW 3.1 Software (Olympus).

Immunofluorescence images of the RNA interference (RNAi) experiment were collected at 0.3-μm increments with an IX-70 microscope (Olympus) and a cooled CCD camera (model CH350; Roper Scientific) controlled by the DeltaVision system (Applied Precision). Images were subjected to deconvolution analysis using the SoftWorx 3.0 program (Applied Precision) as in Nabeshima *et al.* (2005).

For germ cell apoptosis, worms were transferred onto a drop of M9 on 1.5% agarose pads on slides, and assayed using a Hamamatsu Orca II ER/AG camera mounted on a Zeiss ([Carl Zeiss], Thornwood, NY) Axioplan II microscope equipped for fluorescence and DIC.

Small oocyte analyses were performed on 3-day post-L4 adult hermaphrodite whole mounts. Worms were mounted in M9 and extracted gonads were subjected to 3D DIC microscopy (Sulston and Horvitz 1977). Oocytes images were captured and midoocytes plane areas were measured with ImageJ software.

Prophase I-stage nuclei quantification

The number of nuclei at each meiotic stage, from the distal tip to the end of pachytene, was quantified manually on DAPI-stained gonads. The mitotic region was defined from the distal tip of the gonad to the first row of nuclei with clustered chromosome (crescent) morphology. The LZ zone was defined as extending from the first to the last rows, with at least two nuclei having a distinct clustered chromosome morphology. Only nuclei with clustered chromatin were counted to avoid confusion with early pachytene. The pachytene zone was defined as starting at the first row after the LZ zone and extending until diplotene.

Quantitative analysis of germ cell apoptosis

Germ cell corpses were scored in 20-hr post-L4 adult hermaphrodites using acridine orange (AO), as described in Kelly *et al.* (2000). A minimum of 16 gonads were scored for each genotype. For the temperature-sensitivity assays, *mpk-1(ga111)* and wild-type worms were shifted to 25° 4-hr prior to AO incubation. Statistical analyses were performed using the two-tailed Mann–Whitney *U*-test (95% C.I.).

Quantification of immunofluorescence signals

Activated MPK-1 fluorescence intensity was quantified on raw images taken from whole-mounted gonads of wild-type, *ogr-2(huj1)*, *lip-1(zh15)*, and *ogr-2(huj1)*; *lip-1(zh15)* worms stained with an anti-dpMPK-1 antibody, using the same experimental conditions and identical acquisition parameters. ImageJ software was utilized to measure the fluorescence intensity level in a rectangular area at the middle of each meiotic stage.

Time-course analysis for RAD-51 foci

RAD-51 foci were quantified for all seven zones of the gonad, starting with the premeiotic tip to late pachytene regions of the germline, as in Colaiácovo *et al.* (2003), McClendon *et al.* (2016). The total number of nuclei was scored per zone from three gonads, each for wild-type and *ogr-2* mutant worms. The data were also analyzed according to meiotic stages. Statistical comparisons between genotypes were performed using the two-tailed Mann–Whitney *U*-test, 95% C.I.

Quantification of ZHP-3 foci

For quantification of GFP::ZHP3 foci, nuclei that were in the last four-to-five rows of late pachytene and were completely contained within the image stack were analyzed (see *Imaging and microscopy*). Foci were quantified manually from deconvolved 3D stacks.

RNAi

Feeding RNAi experiments were performed at 20°, as described in Govindan *et al.* (2006, 2009). Control RNAi was performed by feeding HT115 bacteria carrying the empty pL4440 vector. A feeding vector from the *C. elegans* RNAi collection (Source Biosciences, Nottingham, UK) was used to deplete *ogr-2* (F52H3.4).

HIM-8 pairing analysis

The gonads were divided into five developmental stages corresponding to the mitotic, LZ, early-, mid-, and late-pachytene stages. Nuclei were scored for HIM-8 foci pairing. Scoring was done similarly to FISH analysis in MacQueen *et al.* (2002), with a 0.7-μm distance between HIM-8 foci used as the cutoff for paired homologous chromosomes.

Quantitative real-time PCR

For quantitative real-time PCR (qRT-PCR), total RNA was isolated from whole worms using Direct-zol Miniprep Plus (Zymo Research), according to the manufacturer's instructions. Worms were subjected to nine rapid freeze–thaw cycles in Trizol (Invitrogen, Carlsbad, CA) prior to RNA isolation. Next, 2 μg of total RNA were reverse-transcribed using SuperScript III Reverse Transcriptase (Invitrogen). Quantitative PCR was performed using Power SYBR Green Mastermix (Applied Biosystems, Foster City, CA) using an Applied Biosystems Step One Plus apparatus (Applied Biosystems). Experiments were performed in triplicate and all data were normalized to *glyceraldehyde 3-phosphate dehydrogenase-1 (gpd-1)*. The primers used were as follows:

lip-1 Forward: 5′-GTG ATT CAG TGA AAC GAG CCA AT-3′.
lip-1 Reverse: 5′-TTG AAC CGC CCA TTA AAC G-3′.
gpd-1 Forward: 5′-ACT CGT CCA TTTT CGA TGC T-3′.
gpd-1 Reverse: 5′-TCG ACA ACA CGG TTC GAG TA-3′.

Data availability

Strains and plasmids are available upon request. Supplemental Material, File S1 contains descriptions of all supplemental figures. File S2 contains detailed descriptions of all primers used for genotyping. Figure S1 contains the sequences for the engineered mutations. Supplemental material available at https://doi.org/10.25386/genetics.7825712.

Results

SPK is a domain, 45 residues in length, which is present in protein kinases of undetermined specificity (STYKc), caspases, SET methyltransferases, and other proteins (Doerks *et al.* 2002). Currently, little is known about this domain beyond its presence in this group of proteins. The domain is present in the N-terminus of the 349-aa protein encoded by F52H3.4, a previously uncharacterized gene expressed in the germline (Reinke *et al.* 2000; Ortiz *et al.* 2014; Diag *et al.* 2018; Tzur *et al.* 2018) (Figure S1A). Below, we describe multiple roles for F52H3.4 in the hermaphrodite adult germline. Accordingly, we renamed this gene *oocyte and germline-related 2* (*ogr-2*).

CRISPR/Cas9-engineered deletions reveal roles for ogr-2 in fertility and prophase I progression

To uncover the genetic roles of *ogr-2* in the germline, we used the CRISPR/Cas9 system (Friedland *et al.* 2013; Chen *et al.*

2014; Paix *et al.* 2015) and isolated two independent null alleles, *ogr-2(huj1)* and *ogr-2(huj18)*, with deletions encompassing the entire *ogr-2* ORF (see *Materials and Methods* and Figure S1, B–D). Both alleles showed similar phenotypes (Figure S2). Unless otherwise specified, all further experiments were conducted using the five-time outcrossed homozygous *ogr-2(huj1)* mutant (hence forward *ogr-2*Δ).

We first determined whether *ogr-2* affects fertility. Worms carrying the *ogr-2(huj1)* allele exhibit a mild, albeit statistically significant, reduction in brood size compared to wild-type (251 ± 25 *vs.* 305 ± 38, $n = 19$ and 20, respectively, see Figure S2). We further monitored embryonic lethality (Emb), a phenotype associated with meiotic defects (as well as other developmental perturbations), and found that it is very slightly increased in *ogr-2*Δ compared to wild-type worms (0.5% ± 0.1 *vs.* 0.2% ± 0.1, $n = 19$ and 20 for *ogr-2*Δ and wild-type, respectively, Figure S2). These results suggest that *ogr-2* may have a role in fertility or development, as well as potential roles in meiosis.

To determine whether *ogr-2* deletion leads to meiotic defects, we examined DAPI-stained mutant gonads. In wild-type young adult hermaphrodite worms, the U-shaped gonads display a highly ordered progression of nuclei [Figure 1A, reviewed in Schvarzstein *et al.* (2010), Lui and Colaiacovo (2013), Pazdernik and Schedl (2013), and Hillers *et al.* (2017)]. We found that the chromatin morphology in most regions of the *ogr-2*Δ gonads is normal; however, we noticed that the relative size of the stages was altered (Figure 1, B–F). More specifically, in *ogr-2*Δ gonads, we found a significant elongation of the mitotic zone. We counted the number of nuclei between the distal tip until the first crescent-like nucleus, which marks the beginning of the first meiotic stage, the LZ stage. We found that the mitotic population is significantly increased in the mutant compared with wild-type worms (260 ± 15 *vs.* 226 ± 16, $n = 8$ and 5, respectively, Figure 1C), indicating that there are more premeiotic nuclei in the *ogr-2* mutant gonads than in the wild-type. To determine whether this increase results from the proliferative nuclei population taking up a larger part of the total number of germ cells, we compared the number of proliferative nuclei relative to the total number of nuclei from the distal tip to the end of pachytene. Indeed, the proliferative nuclei in *ogr-2*Δ compose 0.35 ± 0.03 of this population *vs.* 0.27 ± 0.02 in the wild-type (Figure 1D). We also tested whether this increase is due to a change in the proliferation rate. To this end, we monitored germ cell proliferation by staining the gonads with an antibody against phospho-histone H3 (pH3), a marker of nuclei in M-phase (Hendzel *et al.* 1997; Hans and Dimitrov 2001). We found that the number of pH3-positive nuclei was not significantly higher in *ogr-2*Δ *vs.* wild-type gonads (Figure S3). These results suggest that the lack of OGR-2 increases the size of the mitotic population and that *ogr-2* plays a role in the proper timing of the mitotic-to-meiotic switch.

Our finding that the lack of OGR-2 leads to elongation of the mitotic zone suggests that some regions of prophase I may be shorter. Indeed, although in *ogr-2*Δ the nuclei enter later into the LZ stage and the chromosomes acquire the polarized spatial organization characteristic of this stage, the chromosomes redisperse and adopt a characteristic pachytene morphology earlier, resulting in a significantly shorter LZ zone in *ogr-2*Δ (66 ± 9 $n = 8$) *vs.* wild-type worms (136 ± 20, $n = 6$, Figure 1, E and F). These results suggest that *ogr-2* is involved in leading to timely mitotic-to-meiotic entry and may also play a role in ensuring the correct length of the LZ stage.

Deletion of ogr-2 has a subtle effect on CO designation

Meiotic prophase progression was previously linked to CO control and the formation of bivalent structures at diakinesis (Carlton *et al.* 2006). During the transition from pachytene to diakinesis, several proteins relocalize to specific parts of the chromosome axes (Martinez-Perez and Villeneuve 2005; Nabeshima *et al.* 2005; de Carvalho *et al.* 2008; Martinez-Perez *et al.* 2008; Severson *et al.* 2009; Tzur *et al.* 2012; Severson and Meyer 2014). The axial regions extending from the single chiasma to the farthest end are termed "the long arms" of the bivalents, whereas the regions from the chiasma to the closer end are termed "the short arms" of the bivalents (Figure 2A). During chromosome remodelling, LAB-1 (Long Arms of the Bivalent-1) becomes restricted only to the long arms of the bivalent, thus ensuring that the sister chromatids segregate together at metaphase I (de Carvalho *et al.* 2008). Both *ogr-2*Δ and *ogr-2* RNAi animals exhibited incompletely penetrant chromosome remodeling defects (Figure 2, A and B). RNAi knockdown of *ogr-2* in a strain stably expressing LAB-1, fused to GFP, and mCherry, fused to histone H2B, led to LAB-1 mislocalization in 15% of the oocytes ($n = 20$), where it was present in both the long and short arms of the bivalents (Figure 2A). Similarly, immunostaining using LAB-1 antibodies showed its mislocalization to the short arms of the bivalent in 23% of *ogr-2*Δ oocytes (Figure 2B, $n = 48$–1 oocytes). However, in wild-type worms, LAB-1 was detected only on the long arms ($n = 50$). During this analysis, we also observed that a subpopulation of *ogr-2*Δ −1 oocytes presented one bivalent with a ring shape (Figure 2C). This type of bivalent structure is indicative of double chiasmata created by two COs, which is extremely rare in wild-type worms (Meneely *et al.* 2002; Nabeshima *et al.* 2004; Carlton *et al.* 2006; Lim *et al.* 2008; Martinez-Perez *et al.* 2008; Libuda *et al.* 2013; Gabdank and Fire 2014). In *ogr-2* mutants, we detected bivalents with a ring shape in 6.2% ($n = 48$) of diakinesis nuclei, which we never observed in the wild type ($n = 50$). To verify this result and to determine whether CO designation is perturbed in *ogr-2*Δ, we quantified CO designation levels cytologically. Since *ogr-2* is genomically located near the integration site of the tagged *cosa-1/CNTD1*, an early CO designation marker (Yokoo *et al.* 2012), we were unable to cross the transgene into the *ogr-2* deletion background. Therefore, we used a GFP-tagged ZHP-3/Zip3 strain (Bhalla *et al.* 2008). ZHP-3, a conserved CO-promoting protein, initially localizes in stretches along the full length of the

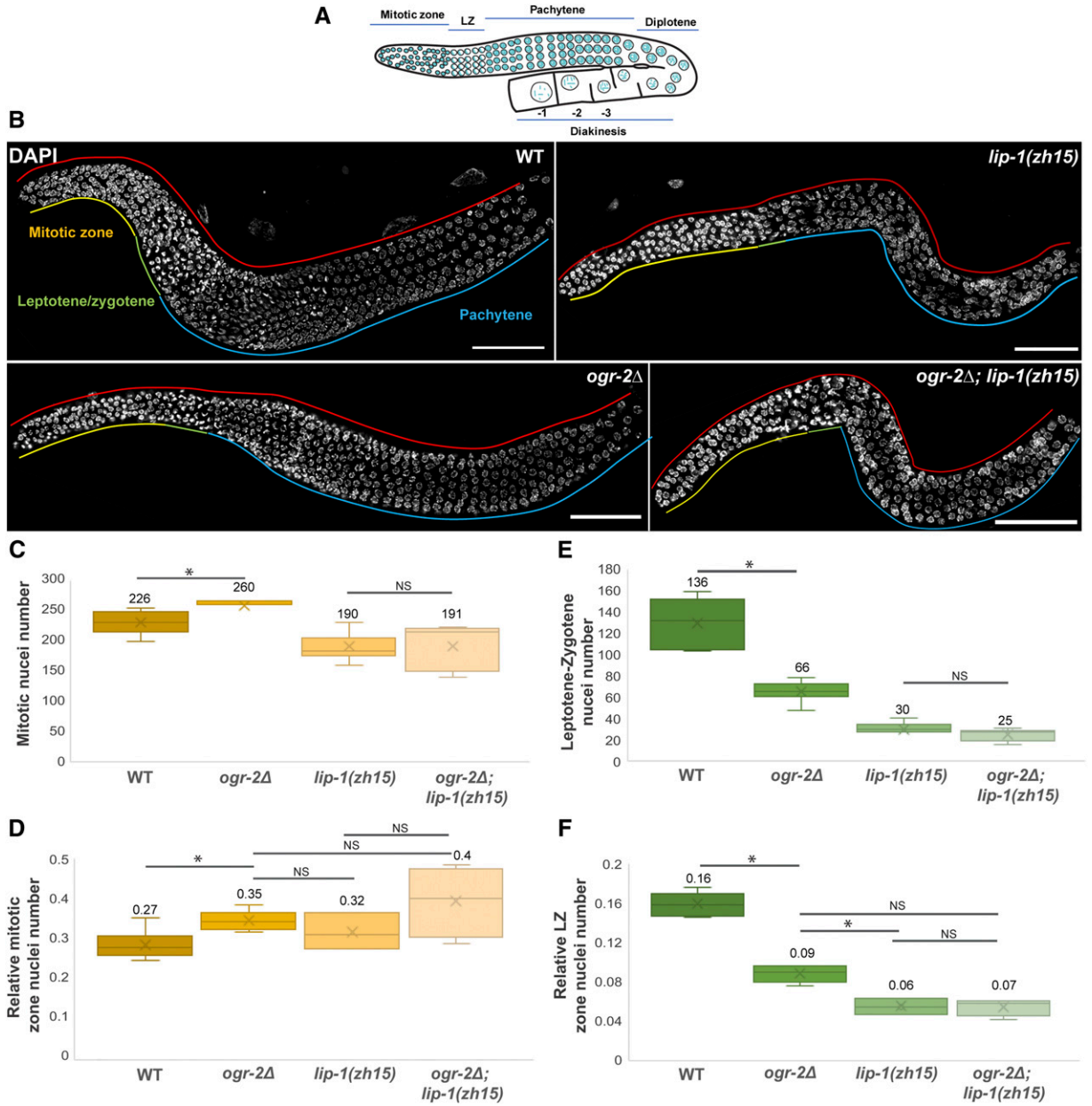

Figure 1 The roles of *ogr-2* and *lip-1* in meiotic progression. (A) An illustration of the *C. elegans* gonad. (B) DAPI staining of WT, *lip-1(zh15)*, *ogr-2*Δ (*ogr-2(huj1)*, a complete deletion of *ogr-2)*, and *ogr-2*; *lip-1(zh15)* gonads. The mitotic zone is denoted by yellow lines, the LZ region by green lines, and pachytene by blue lines. (C–F) Box plots depict the average number of nuclei (C and D) in the mitotic and (E and F) LZ zones. (C and E) The absolute number of nuclei (D and F), the number of nuclei within the indicated zones relative to the total number of nuclei present from the distal tip to the end of pachytene [the red lines in (B)]. Bar, 10 μM. * $P < 0.05$, by two-tailed Mann–Whitney *U*-test. Bars represent the SD. "X" indicates the mean, which is also indicated above each plot. The lengths of the mitotic and LZ zones are significantly altered in the *ogr-2*Δ *gonads*. Note that the *lip-1(zh15)* mutation reduces the total number of germ cells; however, similar changes in the relative size of the mitotic and LZ zones are observed in both mutants. LZ, leptotene/zygotene; NS, not significant; WT, wild-type.

SCs, and then begins to concentrate at one side of each presumptive CO site during late pachytene (Jantsch *et al.* 2004; Bhalla *et al.* 2008). ZHP-3::GFP foci were previously used to quantify CO precursor sites (Bhalla *et al.* 2008; Youds *et al.* 2010; Yokoo *et al.* 2012; Nadarajan *et al.* 2016). In wild-type gonads, we detected six GFP::ZHP3 foci in 93.5% ($n = 139$) of nuclei reflecting a single-CO designation site on each homolog pair (Figure 2, D and E). In contrast, in *ogr-2* mutants, we observed an increase in the number of foci per nucleus (9% of the nuclei had seven GFP::ZHP3 foci *vs.* 0.72% in the wild type, *P*-value < 0.0005 Figure 2, D and E), suggesting a role for OGR-2 in limiting ZHP3-marked CO precursors to one per chromosome pair. Taken together, these results indicate that *ogr-2* plays a role in chromosome remodeling and may also be involved in maintaining tight CO interference.

The SC is properly formed in ogr-2 mutants

During the LZ stage, the SC begins to assemble along the length of the paired chromosomes to keep them closely associated and aligned (Colaiácovo *et al.* 2003; Couteau and Zetka 2005; Hayashi *et al.* 2010; Schild-Prüfert *et al.* 2011). This zipper-like structure is composed of lateral element proteins that are recruited to the chromosome axes and to central region proteins that localize between them [reviewed in Zetka (2009)]. We suspected that in *ogr-2* mutants, the premature redispersion of the nuclei, which denotes the end of the LZ zone, may allow less time for synapsis, resulting in defects in SC assembly. To determine whether SC morphology was altered in *ogr-2*Δ, we performed immunostaining using antibodies against SYP-2, a central region protein (Colaiácovo *et al.* 2003), and HTP-3, an axial component of the SC (MacQueen *et al.* 2002; Goodyer *et al.* 2008; Severson *et al.* 2009). We did not observe any change in the staining of these components between wild-type and *ogr-2*Δ. In wild-type as well as in *ogr-2*Δ pachytene nuclei, both SYP-2 and HTP-3 were colocalized in long contiguous linear stretches between DAPI-stained parallel chromosome tracks, corresponding to fully synapsed homologs (Figure 2F). Similar to SC formation, its disassembly was also normal in *ogr-2*Δ. SYP-2 staining became restricted to the short arms at diplotene and was no longer visible on the −3 oocyte in 80 ($n = 12$) and 83% ($n = 15$) of the oocytes scored for wild-type and *ogr-2*Δ, respectively (Figure 1A). We never found SYP-2 staining on the −2 oocyte. This suggests that *ogr-2* is not required for normal SC assembly and disassembly.

We also evaluated the effect on homologous pairing at the X chromosome pairing centers using HIM-8 antibodies. Pairing at this region was almost identical between *ogr-2*Δ and the wild type. We found 94 ± 6% and 93 ± 5% paired chromosomes in LZ, and 99.8 ± 0.7% and 99 ± 3% in midpachytene, for *ogr-2*Δ and wild-type, respectively (Figure S4). These results indicate that, at least for this chromosomal region, *ogr-2* plays no role in meiotic pairing.

Taken together, these results show that although in *ogr-2* mutants the LZ stage is considerably shorter, at least at this level of cytological observation, *ogr-2* is not required for X chromosome pairing, or for either the formation or the disassembly of the SC.

Deletion of ogr-2 does not lead to a change in the meiotic staging of DSBR

Programmed meiotic DSB formation is initiated at the LZ stage in *C. elegans* (Dernburg *et al.* 1998; Colaiácovo *et al.* 2003). To determine whether this process was affected by the shorter LZ stage, we assessed DSBR progression using an antibody against RAD-51, a protein involved in strand invasion/exchange during DSBR (Rinaldo *et al.* 2002; Alpi *et al.* 2003; Colaiácovo *et al.* 2003). We quantified the number of RAD-51 foci in seven regions from the distal premeiotic tip to the end of pachytene. In young adult wild-type germlines, zones one and two contain mostly premeiotic nuclei, zone three contains mostly LZ nuclei, and zones four-to-seven correspond to progression from early to late pachytene [Figure 3A; Colaiácovo *et al.* 2003; McClendon *et al.* 2016)]. In wild-type worms, the number of RAD-51 foci rose at the end of zone three, peaked in zone four, and dropped in zones five and six, reflecting the progression of DSBR (Figure 3B). In *ogr-2* mutants, we noticed a relative shift in the gonad position regarding the appearance of RAD-51 foci. The number of foci peaked in zone five and only decreased in zone seven (Figure 3B). This shift could be explained by the delay in meiotic onset detected in *ogr-2* mutants. To test this possibility, we reanalyzed our data and binned the nuclei according to their meiotic stage. We found that RAD-51 dynamics during oogenesis were practically identical in *ogr-2*Δ and wild-type worms (Figure 3C). We conclude that *ogr-2* deletion leads to a change in oogenesis progression, which may also lead to a shift in the gonadal position of meiotic stages and thus the position at which DSBR occurs, but it is executed at the correct meiotic stage.

Apoptosis is increased in the ogr-2-deleted worms

Our observation that the number of progeny laid by *ogr-2*Δ mutants is significantly smaller than in wild-type, yet the embryonic lethality is almost indistinguishable from wild-type levels, suggests that many meiocytes are removed by apoptosis. We explored this possibility by scoring the number of apoptotic nuclei by AO staining, taking advantage of its preferential uptake by apoptotic corpses (Mpoke and Wolfe 1997; Gartner *et al.* 2000). In the bend region of wild-type gonads, we counted an average of 3.6 ± 1.6 apoptotic nuclei (Figure 4), which is in line with previous reports [*e.g.*, Lettre *et al.* (2004)]. We found more than a twofold increase in the number of apoptotic corpses in *ogr-2* mutant gonads: 8.1 ± 2.5 (Figure 4).

During oogenesis, stringent quality control systems ensure the production of normal haploid gametes. Checkpoint mechanisms prevent meiotic segregation errors by eliminating defective cells prior to the completion of meiosis (Gumienny *et al.* 1999; Gartner *et al.* 2000; Bhalla and Dernburg 2005). In *C. elegans*, two canonical meiotic checkpoints exist: the synapsis checkpoint and the recombination/DNA damage checkpoint. These checkpoints trigger apoptosis of the affected meiocytes in response to incomplete synapsis and/or unrepaired recombination intermediates in late meiotic prophase (Gartner *et al.* 2000; Bhalla and Dernburg 2005; Woglar *et al.* 2013). In *ogr-2*Δ we detected normal SC formation (Figure 2F) and normal meiotic staging of DSBR (Figure 3C), making this level of increase in apoptosis unexpected. To determine whether the increase in apoptosis is related to DSBR or synapsis, we utilized the *syp-1(me17)* mutation, where both synapsis and DSBR checkpoints are activated, leading to a large number of apoptotic nuclei (MacQueen *et al.* 2002; Ye *et al.* 2014). If the increase in apoptosis observed in *ogr-2*Δ is due to the canonical checkpoints (either DSBR or synapsis), we would expect no additive effect of these two pathways in the double mutant of *ogr-2* and *syp-1* worms. On the other hand, if the increase in

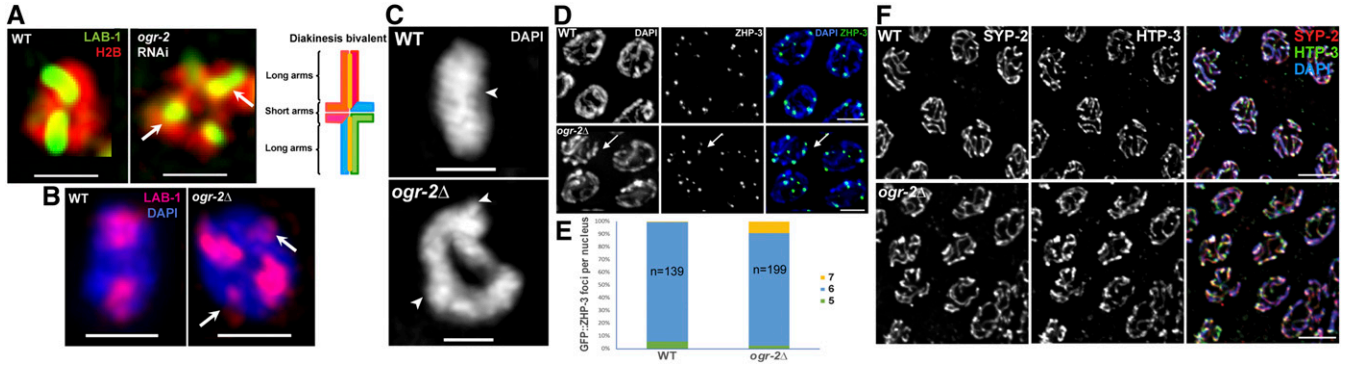

Figure 2 Deletion of *ogr-2* leads to the formation of aberrant bivalent structures and increased ZHP-3 foci with normal SC formation. (A) Images of bivalents in diakinesis oocytes with mCherry-tagged histone H2B and GFP-tagged LAB-1 of control and *ogr-2* RNAi worms. (B) Immunostaining for LAB-1 in a bivalent of a diakinesis oocyte in WT and *ogr-2*Δ gonads. Red: LAB-1. Blue: DAPI. Arrows: LAB-1 mislocalization to the short arms. Bar, 1 μM. (C) DAPI staining of bivalents in diakinesis nuclei. In total, 6.2% of *ogr-2*Δ nuclei contain a bivalent with a ring shape (depicted). Arrowheads point toward chiasmata. Bar, 1 μM. (D) Representative images of gonads with ZHP-3 foci (green) stained with DAPI (blue) from late-pachytene nuclei in WT and *ogr-2*Δ mutants. Arrows indicate a nucleus with seven foci. Bar, 5 μM. (E) Distribution of the percentage of ZHP-3 foci per late-pachytene nucleus. Note the increase in seven foci in *ogr-2*Δ. (F) Pachytene nuclei immunostained for SYP-2 (red) and HTP-3 (green). Bar, 4 μM. RNAi, RNA interference; SC, synaptonemal complex; WT, wild-type.

apoptosis in *ogr-2*Δ is not due to activation of these checkpoints, but rather is due to a different mechanism, then the double mutant should display an additive effect.

In *syp-1* mutants, we scored an average of 15.8 ± 2.6 apoptotic nuclei per gonad arm, which is in line with previous reports (Ye *et al.* 2014). In the *ogr-2*; *syp1* double mutant, we found a significant increase in the number of apoptotic nuclei (18.8 ± 3.7, Figure 4). We note that the increase in apoptotic nuclei in the double mutant is less than the complete additive values of the single mutants. We hypothesize that this incomplete additive value stems from the high apoptotic levels, which may be close to the limit of the neighboring cells' ability to process all the apoptotic nuclei with the same dynamics. We can conclude that this increase in germline apoptosis is consistent with a possible role that is independent of synapsis and DSBR.

To verify that the increase in apoptosis is not due to unrepaired DSBs, we quantified the number of apoptotic nuclei in a *hus-1*-mutant background. It was previously shown that HUS-1 is a DNA damage checkpoint protein and that DNA damage-induced germ cell death is abrogated in *hus-1* mutants. Highly reduced levels of germ cell apoptosis are detected in *hus-1* mutants following treatment with ionizing radiation (Hofmann *et al.* 2002; Quevedo *et al.* 2007). If the increased apoptosis in *ogr-2*Δ is due to unrepaired DSBs, then the *hus-1*; *ogr-2*Δ double mutant is expected to exhibit a lower number of apoptotic nuclei. Alternatively, if the increased apoptosis in *ogr-2*Δ is unrelated to DSB repair, then the *hus-1* mutation in *ogr-2*Δ should not alter the level of apoptosis. We found 7.6 ± 1.7 apoptotic nuclei in gonads of *ogr-2*Δ *hus-1*, which is not significantly different from the levels found in *ogr-2*Δ (see above; Figure 4). We can conclude that the increased apoptosis in *ogr-2*Δ is not due to unrepaired DSBs.

MAPK, through MPK-1/ERK, was shown to increase germline apoptosis independently of the synapsis and recombination/DNA damage checkpoints (Schumacher *et al.* 2001; Rutkowski *et al.* 2011) by directly interacting with CEP-1, the *C. elegans* p53 homolog (Derry *et al.* 2001; Rutkowski *et al.* 2011). We investigated whether the *ogr-2*Δ increased apoptosis is MPK-1-dependent. To this end, we eliminated MAPK signaling in *ogr-2* mutants by combining it with the temperature-sensitive mutant *mpk-1(ga111ts)*. This mutation is a weak temperature-sensitive loss-of-function allele that reduces the rate of activation and phosphorylation of MPK-1 (Lee *et al.* 2007b). At a restrictive temperature (25°), the number of apoptotic nuclei in the bend region of the germline in the *ogr-2*; *mpk-1* double mutant was significantly lower than in *ogr-2*Δ (3.4 ± 1.5, Figure 4) and was indistinguishable from *mpk-1(ga111ts)* (3.7 ± 1.6). Thus, the *mpk-1* mutation suppresses the increase in germ cell apoptosis observed in *ogr-2*Δ. These results are consistent with our hypothesis that the elevated level of apoptosis in *ogr-2* mutants is dependent on MPK-1/ERK activation, but not on the synapsis and recombination checkpoints.

It has been previously reported that activation of MPK-1 in diplotene increases apoptosis through CEP-1 (Lee *et al.* 2007b; Rutkowski *et al.* 2011). Therefore, we investigated whether the aberrant rise in apoptosis found in *ogr-2* mutants is CEP-1-dependent. In *cep-1*; *ogr-2* double mutants, the enhanced apoptosis was suppressed (2.5 ± 1.9 for *cep-1*; *ogr-2*Δ and 1.6 ± 1.6 for *cep-1*, Figure 4). The dependence of *ogr-2* apoptotic control on *cep-1* once again supports our conclusion that OGR-2 apoptotic control is dependent on MPK-1.

Inactivation of LIP-1 leads to an increase in germline apoptosis by relieving the negative regulation of MAPK signaling (Hajnal and Berset 2002; Rutkowski *et al.* 2011). Therefore, we investigated whether *ogr-2* apoptotic control operates via the same pathway as *lip-1*. We found that *ogr-2*; *lip-1(zh15)* double mutants did not display an additive increase in germline apoptosis over *lip-1(zh15)* (11 ± 3 *vs.*

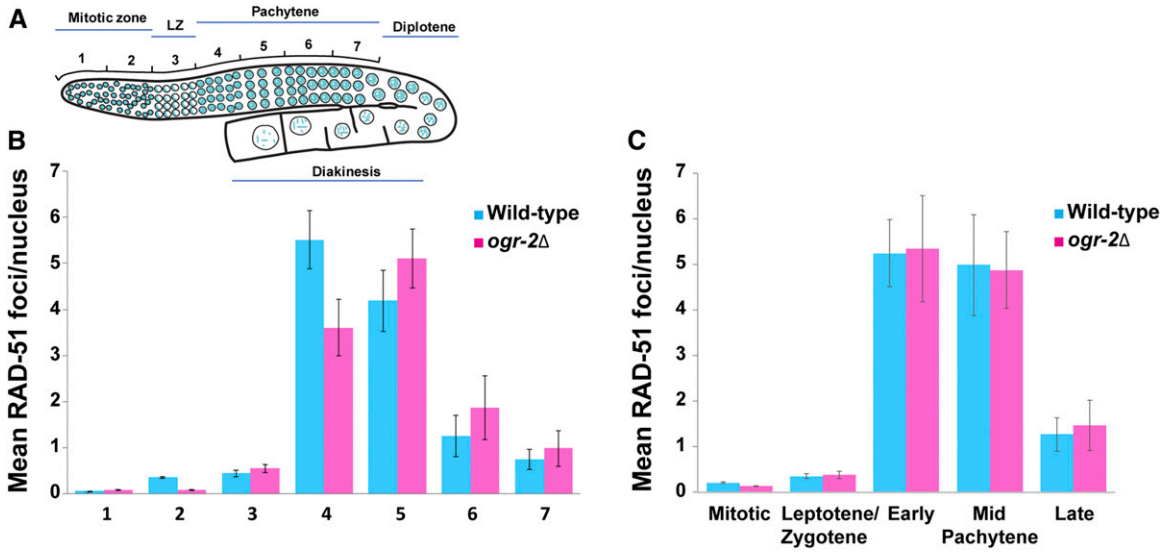

Figure 3 Double-strand break repair position in *ogr-2*Δ. Double-strand break repair quantification by immunostaining of RAD-51. (A) Illustration of the *C. elegans* gonad. The zones of RAD-51 analysis are depicted. (B) Mean foci/nuclei in the seven equally divided zones from the premeiotic tip to late pachytene. (C) The same analysis binned according to developmental stages. Bars represent the SD. LZ, leptotene/zygotene.

10 ± 2 for *ogr-2*Δ; *lip-1(zh15)* and *lip-1(zh15)*, respectively, Figure 4). We can conclude that *ogr-2* restricts germline apoptosis through *mpk-1* and possibly *lip-1*.

*Increased MPK-1 activation in ogr-2*Δ

Previous studies indicated that *LIP-1*-mediated dephosphorylation deactivates MPK-1 in diplotene and, consequently, worms carrying a *lip-1* loss-of-function mutation had elevated MPK-1 activity in this region, resulting in increased apoptosis (Hajnal and Berset 2002; Rutkowski *et al.* 2011). We tested the hypothesis that OGR-2 affects the proper spatial activation of MPK-1, similar to LIP-1, by assessing the localization pattern of the MPK-1 active form, *i.e.*, dpMPK-1 in *ogr-2* mutant germlines. Staining of wild-type gonads using an antibody directed against dpMPK-1 recapitulated the previous results. Two main activation regions of MPK-1 were found: the region that spans mid-to-late pachytene and a proximal region of activation in diakinesis oocytes [reviewed in Arur (2017); Figure 5A]. At other stages of the gonad, the staining was very weak (Lee *et al.* 2007a,b; Yin *et al.* 2016). Unlike in wild-type worms, dpMPK-1 staining persists in the diplotene region of *ogr-2* gonads, similar to *lip-1(zh15)* mutants (Figure 5A; Hajnal and Berset 2002; Rutkowski *et al.* 2011). These results suggest that *ogr-2* plays a role in limiting MPK-1 activation in the diplotene stage; thus, it regulates apoptosis levels.

To better characterize the effects of *ogr-2* on MPK-1 activation, we quantified the intensity of dpMPK-1 staining along the different gonad regions. We detected a significant ectopic activation of MPK-1, not only in diplotene, but also in the mitotic and LZ zones of *ogr-2*Δ gonads (Figure 5B). Thus, *ogr-2* is involved in reducing MPK-1 activation along most of the adult gonad. The correlation between the regions in *ogr-2*Δ gonads where MPK-1 was aberrantly activated and where meiotic progression was abnormal suggests that OGR-2 meiotic control acts via restriction of MPK activation (see the *Discussion*).

Mutations in lip-1 and ogr-2 result in similar defects in oocyte morphology and MPK-1 activation

In both *lip-1* and *ogr-2*Δ, aberrant apoptotic control exists and dpMPK-1 persists in diplotene. This raises the hypothesis that they may also act at other meiotic stages via the same pathway. To test that possibility, we quantified the relative dpMPK-1 staining in *lip-1* gonads. Interestingly, higher activation levels were observed not only in diplotene but also in the mitotic and LZ stages, almost identically to *ogr-2*Δ (Figure 5B). However, this aberrant activation was not additive. Indeed, in the double mutant *ogr-2*; *lip-1*, we found no statistically significant differences in dpMPK-1 staining compared with the single mutants; however, in all three strains we measured significantly higher dpMPK-1 levels than in the wild type (Figure 5B).

The activation of MPK-1 in *lip-1* and *ogr-2* was accompanied by almost identical changes in meiotic progression in the two mutants. In the early stages of *lip-1(zh15)* gonads, we found relative elongated mitotic zones and shorter LZ zones, very similar to the *ogr-2*Δ gonads. These changes were not additive, since in the double mutant we found a similar relative nuclei number compared to the single mutants (Figure 1, D and F), indicating that they work through the same pathway.

Similarities also exist between the fates of mature oocytes in *ogr-2*Δ and *lip-1(zh15)* mutants (Figure 6, A–I). Three-day-old *lip-1(zh15)* mutants exhibit a defective G2/M-phase arrest, with endomitotic germ cells and smaller oocytes aligned in multiple rows owing to aberrant oocyte maturation (Hajnal and Berset 2002). Using DIC optics, we measured the

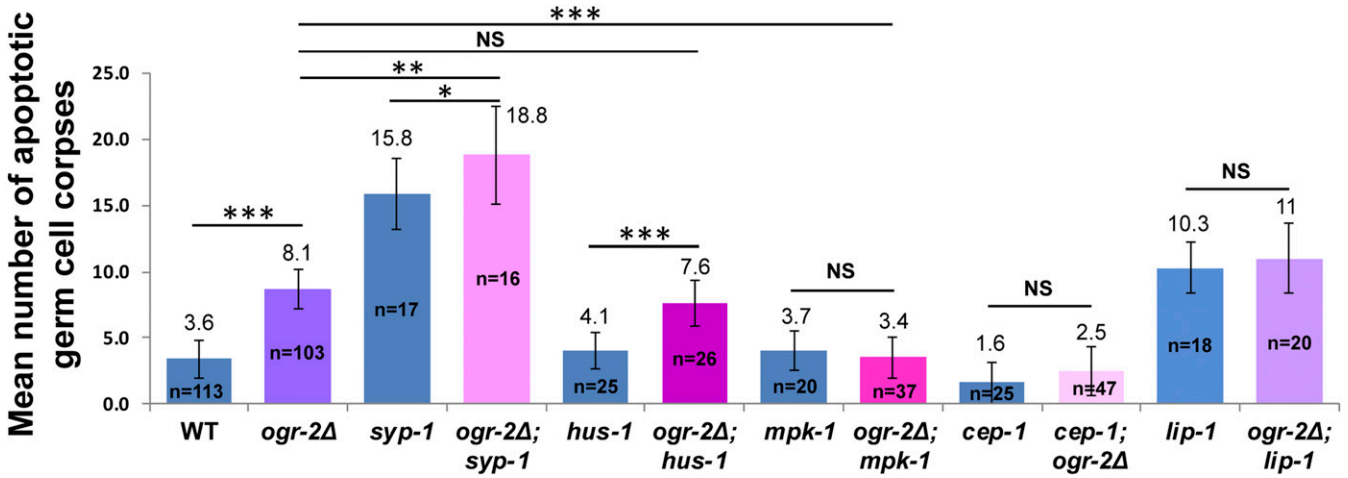

Figure 4 Elevated apoptosis levels in *ogr-2* mutants are dependent on MPK-1, but not on DSBR and synapsis. Quantification of germline apoptosis by acridine orange staining. * $P < 0.05$, *** $P < 0.0001$ by the two-tailed Mann–Whitney *U*-test. Bars represent the SD. Deletion of *ogr-2* leads to an increase in apoptosis, which is partially additive when combined with *syp-1* mutation but is blocked by mutation in *mpk-1*. DSBR, double-strand break repair; NS, not significant; WT, wild-type.

size of mature oocytes and found that, in both *ogr-2*Δ and *lip-1(zh15)*, they were significantly smaller than in wild-type worms (Figure 6, F–I). In line with these results, DAPI staining indicated that oocytes in both *ogr-2*Δ and *lip-1(zh15)* were often aligned in multiple rows (41.2%, $n = 17$ and 100%, $n = 7$, respectively, Figure 6, B and D). Moreover, in the gonads of both genotypes we found endomitotic nuclei strongly stained with DAPI (41.2%, $n = 17$ in *ogr-2*Δ *vs.* 28.5%, $n = 7$ in *lip-1(zh15)*, Figure 6, C and E). These two phenotypes were never observed in the gonads of wild-type worms of the same age ($n = 15$, Figure 6A). The changes we found in oocyte morphology were not due to the lack of sperm, since we found a similar number of sperm in *ogr-2*Δ and wild-type gonads (131 ± 25 in *ogr-2*Δ *vs.* 127 ± 22 in wild-type in day 1 adult worms, and 3 ± 3 in day 3 adult worms for both).

The elevated level of activated MPK-1 in *lip-1(zh15)* was previously shown to relieve some of the phenotypes observed in temperature-sensitive mutations in *mpk-1* (Hajnal and Berset 2002). We investigated whether the deletion of *ogr-2* can result in the same outcome. When *mpk-1(ga111ts)* worms were shifted to the restrictive temperature, very few progeny were observed (6 ± 2 per worm, $n = 49$). Similar to previous results (Hajnal and Berset 2002), we found that a mutation in *lip-1* partially relieved this effect (22 ± 5 per worm, $n = 30$). In *ogr-2*; *mpk-1* double mutants, we also found a significantly greater number of progeny (47 ± 9, $n = 30$, *P*-value < 0.00001 by the two-tailed Mann–Whitney *U*-test, compared with *mpk-1*). Thus, mutations in *lip-1* and *ogr-2* lead to similar effects on apoptosis, MPK-1 activation, and oocyte maturation, and both partially suppress the effects of *mpk-1(ga111ts)* mutation.

OGR-2 localizes to chromatin and may act to enhance lip-1 transcription

To gain insight into the mechanism by which *ogr-2* acts to restrict the activation of MPK-1 via *lip-1*, we used CRISPR engineering to insert a triple FLAG-tag before the STOP codon of the endogenous *ogr-2* gene to create the OGR-2-tagged version strain, YBT44. After staining gonads of this strain with anti-FLAG antibodies, we observed an OGR-2-FLAG signal on the chromatin of all nuclei in the gonad (Figure 7). This signal was not detected in wild-type gonads (Figure S5). Interestingly, at higher magnification, stronger OGR-2-FLAG signals were observed as foci and patches on chromatin, and became stronger during mid/late pachytene (Figure 7).

It was previously reported that LIP-1 localizes as distinct cytoplasmic puncta during pachytene (Hajnal and Berset 2002). The increased OGR-2 chromatin-associated staining during mid/late pachytene, at the same region where dpMPK-1 staining becomes stronger, raised the hypothesis that OGR-2 acts in the nucleus to enhance *lip-1* expression. To test this hypothesis, we quantified *lip-1* mRNA levels by qRT-PCR. Importantly, we found that the levels were reduced by 40% in *ogr-2*Δ *vs.* wild-type (Figure 6J). We conclude that OGR-2 is present in germline nuclei, where it acts to maintain normal levels of *lip-1* mRNA.

Discussion

Successful gametogenesis requires the concerted execution of complex cellular processes within the context of a viable organ. We show here that oogenesis coordination, ranging from proliferation to the mature oocyte, is skewed in a strain with complete deletion of *ogr-2*. Without *ogr-2*, entry into meiosis is delayed, the LZ stage is shorter, and the apoptosis rates are elevated (Figure 1 and Figure 4). One caveat that must be considered is that due to the similarities between LZ and early pachytene morphologies, the purity of the scored LZ population may be incomplete. In *ogr-2*Δ gonads, proper chromosome remodeling fails and low levels of bivalents with double chiasmata are present (Figure 2). We also found

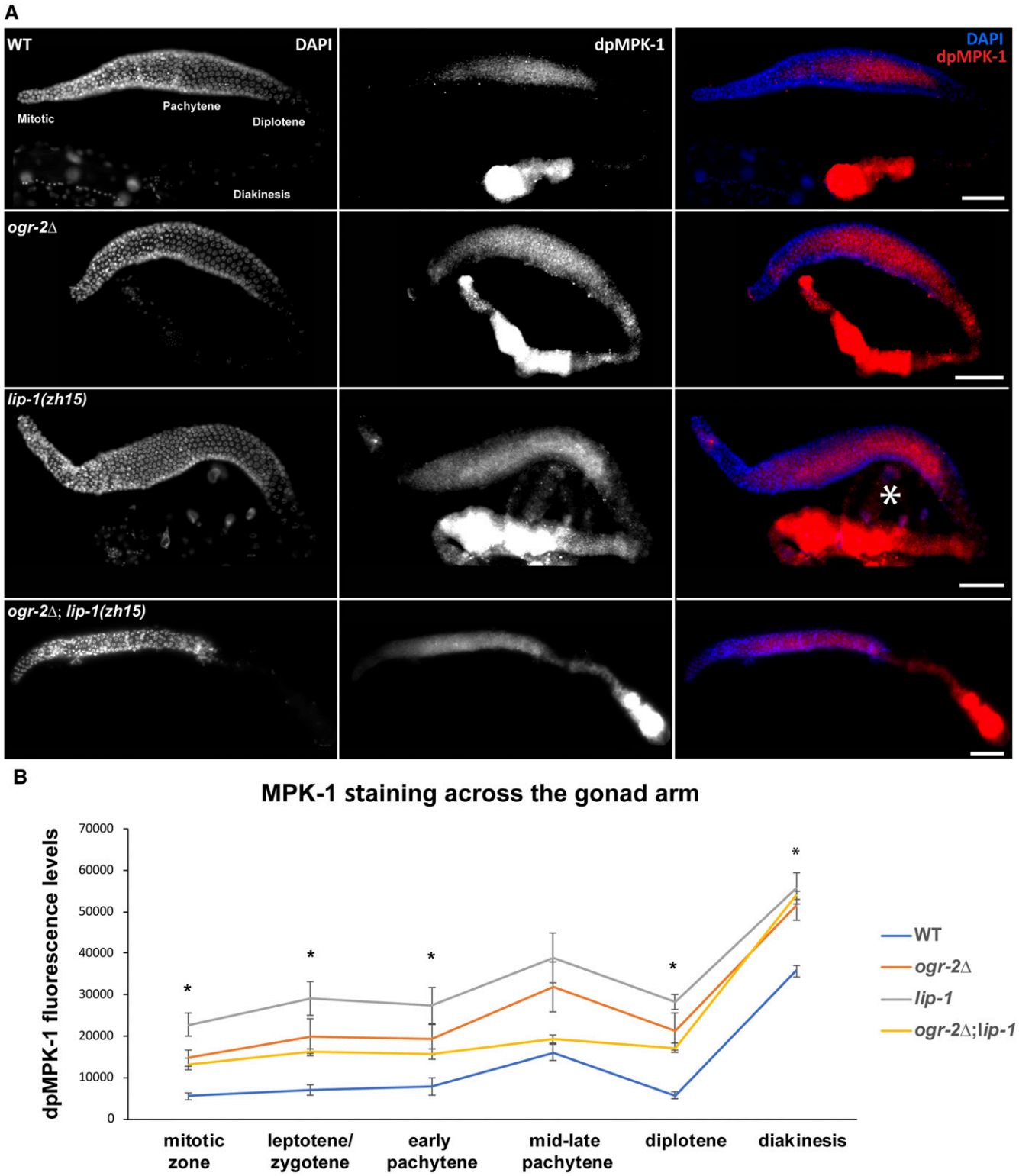

Figure 5 Aberrant MPK-1 activation regions in *ogr-2*Δ. (A) Immunostaining of activated MPK-1 (dpMPK-1) in WT, *ogr-2*Δ, *lip-1(zh15)*, and *ogr-2*Δ; *lip-1(zh15)* gonads. Note the aberrant staining at early stages and at diplotene present in *ogr-2*Δ, *lip-1*, and *ogr-2*Δ; *lip-1*. Nonrelated gut nuclei are denoted by an asterisk. (B) Quantification of the dpMPK-1 intensity. Bars represent SEM. Asterisks indicate $P < 0.05$ by the two-tailed Mann–Whitney *U*-test for all mutants compared to WT. dpMPK-1, double-phosphorylated MPK-1; WT, wild-type.

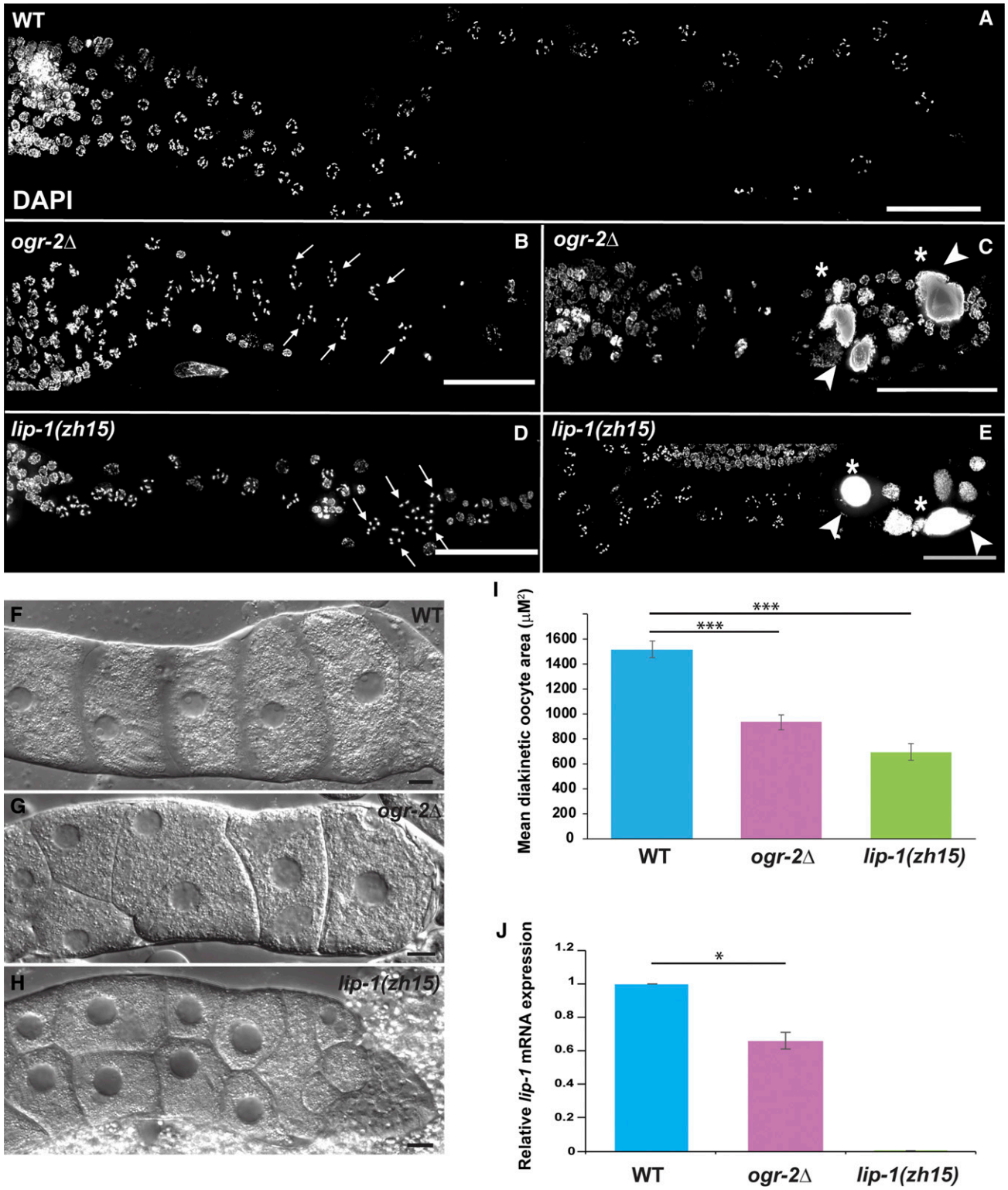

Figure 6 Interactions and similarities between *ogr-2*Δ and *lip-1*. DAPI-stained gonads of (A) wild-type (WT), (B and C) *ogr-2*Δ, and (D and E) *lip-1(zh15)*. Bar, 50 μM. Arrows indicate oocytes stacked in pairs. Arrowheads indicate endomitotic nuclei in which the acquisition was oversaturated to facilitate the observation of both endomitotic and meiotic nuclei. (F–H) Images using DIC optics of dissected gonads of (F) N2, (G), *ogr-2*Δ, and (H) *lip-1(zh15)*. (I) Quantification of oocyte size. *** $P < 0.001$ using the two-tailed Mann–Whitney *U*-test. (J) Real-time PCR analysis of *lip-1* expression. * $P < 0.05$ using the two-tailed Mann–Whitney *U*-test.

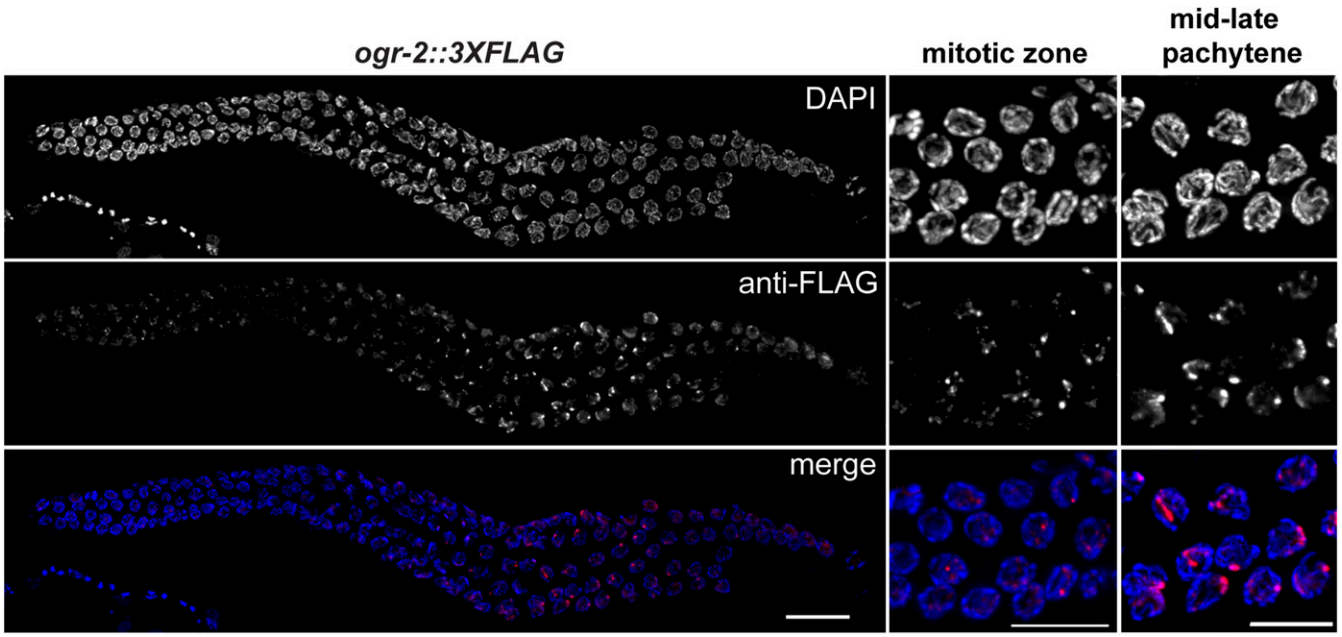

Figure 7 OGR-2 is present on germ cell chromatin. Gonad of *ogr-2*::*3XFLAG* stained with DAPI and anti-FLAG antibody. Bar for whole mount, 20 μM. Bar for mitotic zone and midlate pachytene, 10 μM.

age-dependent aberrations in oocyte morphology in *ogr-2*Δ and stacked oocytes entering endomitosis without fertilization (Figure 6). The aberrant developmental progression and high apoptosis levels probably lead to the lower numbers of progeny observed in these worms. Concurrent with the developmental changes observed in this strain, we found that MPK-1 activation is elevated in *ogr-2*Δ gonads in the proliferative, LZ, and diplotene stages; we propose that this increase is the source of many of the observed meiotic alterations (discussed next).

The roles of ogr-2 in attenuating MPK-1 activation

Oogenesis, like many other developmental and differentiation processes, is orchestrated by executing a genetic program that is activated by intra- and internuclei signaling. MAPK signaling has been found to be involved in many processes throughout oogenesis, ranging from yeast to mouse (Zhang *et al.* 2010; Sukegawa *et al.* 2011; Nabti *et al.* 2014; Arur 2017). In *C. elegans*, where oogenesis is continuous, MAPK signaling is required for meiotic coordination and, when it is blocked, the program fails and the nuclei are arrested at the end of pachytene (Church *et al.* 1995). The model in which MAPK signaling facilitates oogenesis progression is supported by the activation and deactivation of MPK-1 at different parts of the gonad, a switch that was shown to regulate sets of genes required for meiotic coordination (Leacock and Reinke 2006; Lin and Reinke 2008; Arur 2017). Mutations that affect MPK-1 activation result in aberrations during nearly every stage of this developmental program (Gumienny *et al.* 1999).

The deletion of *ogr-2* leads to higher levels of MPK-1 activation in many regions including the mitotic and the LZ regions, as well as during the diplotene stage (Figure 5). Comparable to other mutations that change MAPK signaling, this deletion also results in meiotic progression phenotypes at many stages. These include delayed meiotic entry, elevated apoptosis levels, altered chromosome remodelling, and endomitosis (Church *et al.* 1995; Hajnal and Berset 2002; Lee *et al.* 2006, 2007a; Yin *et al.* 2016). Surprisingly, the meiotic changes in *ogr-2*Δ only slightly affect embryonic lethality. We speculate that this is due to the high level of apoptosis, which removes most of the affected nuclei. The elevated apoptosis levels were MPK-1-dependent, supporting our conclusion that the *ogr-2*Δ germline phenotypes at least partly result from the elevated activation levels of MPK-1.

The model that emerges from these results is that OGR-2 attenuates MPK-1 activation levels, keeping them low before midlate pachytene and during diplotene, to allow the timely execution of meiosis. When OGR-2 is not present, entry into meiosis is delayed, which probably allows less time for recombination. It is possible that the aberrations we observed at the late stages in *ogr-2*Δ gonads, which include altered chromosome remodelling and chiasmata levels, are the secondary outcome of earlier events. Alternatively, these defects could directly result from the elevated MAPK signaling at these later stages, since numerous studies showed that correct MPK-1 activation is required for the last steps of prophase I (Church *et al.* 1995; Hajnal and Berset 2002; Lee *et al.* 2007a,b; Arur *et al.* 2009).

Does OGR-2 affect germline development through LIP- 1?

Other proteins were previously shown to control meiotic progression by restricting the extent of MPK-1 activation. For example, a mutation in *kin-18* leads to "flickering"

MPK-1 activation from the early-to-late oogenesis stages. These regions of activation encompass different numbers of nuclei (Yin *et al.* 2016). These worms have a mixture of pachytene and diakinesis nuclei, and nuclei with late prophase I chromosome morphology are present at distal parts of the gonad. In *kin-18* mutant gonads, RAD-51 and COSA-1 foci appear much earlier (Yin *et al.* 2016). Mutations in the germinal center kinase gene *gck-1* lead to increased staining of activated MPK-1 in pachytene. This results in fewer germ cells, higher apoptotic levels, small oocytes, and nuclei with an undefined chromatin morphology (Schouest *et al.* 2009). These mutations indicate that correct MPK-1 activation along the gonad is a prerequisite for proper oogenesis progression.

One of the best-characterized regulators of MPK-1 is LIP-1. Similar to other genes that affect MPK-1 activation, *lip-1* is also required for normal oogenesis progression, germline proliferation, and oocyte maturation (Hajnal and Berset 2002; Lee *et al.* 2006; Rutkowski *et al.* 2011; Cha *et al.* 2012). Several lines of evidence support a common pathway for *lip-1* and *ogr-2* in controlling meiotic progression through MPK-1 deactivation: (1) in both mutants there is a similar change in the spatial activation of MPK-1, and it is present in the mitotic and diplotene regions (Figure 5); (2) both are involved in maintaining the relative size of the mitotic and LZ populations (Figure 1); (3) in mutants of both genes, there is increased apoptosis in the bend region, which is not dependent on recombination or synapsis checkpoints (Rutkowski *et al.* 2011; Figure 4); (4) both play a role in oocyte maturation and G2/M transition block prior to fertilization (Hajnal and Berset 2002; Figure 6) in older hermaphrodites; and (5) mutations in both genes can relieve the sterility of *mpk-1* temperature-sensitive alleles [this work and Hajnal and Berset (2002)]. Interestingly, *lip-1* and *ogr-2* transcripts were found to be associated with both FBF-1 and FBF-2 (Lee *et al.* 2006; Prasad *et al.* 2016), two partially redundant proteins expressed at the distal part of the gonad following GLP-1/Notch signaling. The FBF proteins reduce the stability and translation efficiency of hundreds of transcripts to maintain the proliferative population (Prasad *et al.* 2016). Thus, the same mechanism probably prevents the expression of *lip-1* and *ogr-2* distally to maintain the proliferative population. The common phenotypes of *lip-1* and *ogr-2*Δ suggest that *ogr-2* is part of the same pathway that utilizes the phosphatase LIP-1 to restrict the activation of MPK-1; thus, *ogr-2* coordinates oogenesis progression. We note that some phenotypes are not shared between the mutants. For example, LAB-1 is not mislocalized in *lip-1* mutants (Nadarajan *et al.* 2016), as it is in the minority of *ogr-2* diakinesis bivalents (Figure 3, A and B). On the other hand, in *lip-1* mutants, defects exist in SC disassembly (Nadarajan *et al.* 2016); these defects are not observed in *ogr-2* mutants (this study). In addition, *lip-1* has ∼50% embryonic lethality (Hajnal and Berset 2002), compared with only 0.5% in *ogr-2*Δ. We hypothesize that this could result from the following: (1) the MPK-1-independent roles of LIP-1; (2) the roles of OGR-2, which are mediated through other pathways; or (3) the partial effect of OGR-2 on LIP-1 (Figure 6J).

How can OGR-2 promote LIP-1 activity? To the best of our knowledge, the function of the SPK domain has not yet been resolved, but since it is also present in proteins that are part of chromatin-modifying complexes (Doerks *et al.* 2002), one attractive possibility is that OGR-2 is part of such a complex. This possibility is supported by the presence of OGR-2 on the chromatin in foci and patches (Figure 7), and it can explain how *ogr-2* promotes *lip-1* expression through transcriptional regulation. This regulation could either affect *lip-1* directly or it could act through genes upstream of *lip-1*, such as *dpl-1* or *efl-1* (Lin and Reinke 2008). This possibility can also explain why we failed to find additive effects in the *lip-1* and *ogr-2* double mutant for most of the phenotypes tested (Figure 1, Figure 4, and Figure 5), and why sometimes the *ogr-2*Δ phenotype is milder than the *lip-1* phenotype. If a lack of *ogr-2* affects a chromatin modifier complex, it is expected to influence the expression of many genes, which would explain why some of the *ogr-2* phenotypes are not shared with *lip-1* (as mentioned before). In the future, it would be interesting to determine which proteins interact with OGR-2. Note that we measured only a 40% reduction of *lip-1* in *ogr-2*Δ worms, while to the best of our knowledge no haploinsufficiency was reported for *lip-1* mutants, yet there are still similar phenotypes in *lip-1* and *ogr-2*Δ. We believe that this can be explained by the fact that we measured *lip-1* levels in mixed populations of whole worms, whereas OGR-2 may play specific roles in the gonad.

Most of the data presented here suggest that OGR-2 functions by reducing MPK-1 activation. Nevertheless, it is also possible that OGR-2 plays MPK-1-independent meiotic roles that remain to be defined. Genetic interactions suggest that OGR-2 attenuates MAPK signaling via LIP-1. We note that in both mutants the increased MPK-1 activation (as observed by dpMPK-1 staining) is less than an order of magnitude greater than in wild-type worms. Nevertheless, the effects of this mild difference are evident in several oogenesis stages, highlighting the importance of accurate MAPK signaling. It is possible that small changes in MAPK activation are amplified to other local and global signaling molecules and effectors, and, if so, the outcome is detrimental. Spatial proteomics analyses in the gonad will advance our understanding of how oogenesis is coordinated in the syncytial environment of the worm's gonad. Applying these future tools in *lip-1* and *ogr-2*Δ gonads would help reveal the effects that small changes in MAPK signaling induce, as well as how this controls meiotic progression at each step.

Acknowledgments

We thank the *Caenorhabditis* Genetics Center, Anne Villeneuve, and Sarit Smolikove for kindly providing strains; Monique Zetka for the HTP-3 antibody; and Sarit Smolikove for the SYP-2 antibody. This work was supported by Israel Science Foundation grants 1283/15 and 2090/15, and a

European Commission Individual Fellowship (H2020-MSCA-IF grant 654853) to Y.B.T., and by National Institutes of Health grant R01 GM-072551 to M.P.C.

Literature Cited

Alpi, A., P. Pasierbek, A. Gartner, and J. Loidl, 2003 Genetic and cytological characterization of the recombination protein RAD-51 in Caenorhabditis elegans. Chromosoma 112: 6–16. https://doi.org/10.1007/s00412-003-0237-5

Arur, S., 2017 Signaling-mediated regulation of meiotic prophase I and transition during oogenesis. Results Probl. Cell Differ. 59: 101–123. https://doi.org/10.1007/978-3-319-44820-6_4

Arur, S., M. Ohmachi, S. Nayak, M. Hayes, A. Miranda *et al.*, 2009 Multiple ERK substrates execute single biological processes in Caenorhabditis elegans germ-line development. Proc. Natl. Acad. Sci. USA 106: 4776–4781. https://doi.org/10.1073/pnas.0812285106

Bhalla, N., and A. F. Dernburg, 2005 A conserved checkpoint monitors meiotic chromosome synapsis in Caenorhabditis elegans. Science 310: 1683–1686. https://doi.org/10.1126/science.1117468

Bhalla, N., D. J. Wynne, V. Jantsch, and A. F. Dernburg, 2008 ZHP-3 acts at crossovers to couple meiotic recombination with synaptonemal complex disassembly and bivalent formation in C. elegans. PLoS Genet. 4: e1000235 (erratum: PLoS Genet. 4). https://doi.org/10.1371/journal.pgen.1000235

Brenner, S., 1974 The genetics of Caenorhabditis elegans. Genetics 77: 71–94.

Carlton, P. M., A. P. Farruggio, and A. F. Dernburg, 2006 A link between meiotic prophase progression and crossover control. PLoS Genet. 2: e12. https://doi.org/10.1371/journal.pgen.0020012

Cha, D. S., U. S. Datla, S. E. Hollis, J. Kimble, and M. H. Lee, 2012 The Ras-ERK MAPK regulatory network controls dedifferentiation in Caenorhabditis elegans germline. Biochim. Biophys. Acta 1823: 1847–1855. https://doi.org/10.1016/j.bbamcr.2012.07.006

Chen, X., F. Xu, C. Zhu, J. Ji, X. Zhou *et al.*, 2014 Dual sgRNA-directed gene knockout using CRISPR/Cas9 technology in Caenorhabditis elegans. Sci. Rep. 4: 7581. https://doi.org/10.1038/srep07581

Chen, Z., T. B. Gibson, F. Robinson, L. Silvestro, G. Pearson *et al.*, 2001 MAP kinases. Chem. Rev. 101: 2449–2476. https://doi.org/10.1021/cr000241p

Church, D. L., K. L. Guan, and E. J. Lambie, 1995 Three genes of the MAP kinase cascade, mek-2, mpk-1/sur-1 and let-60 ras, are required for meiotic cell cycle progression in Caenorhabditis elegans. Development 121: 2525–2535.

Colaiácovo, M. P., A. J. MacQueen, E. Martinez-Perez, K. McDonald, A. Adamo *et al.*, 2003 Synaptonemal complex assembly in C. elegans is dispensable for loading strand-exchange proteins but critical for proper completion of recombination. Dev. Cell 5: 463–474. https://doi.org/10.1016/S1534-5807(03)00232-6

Couteau, F., and M. Zetka, 2005 HTP-1 coordinates synaptonemal complex assembly with homolog alignment during meiosis in C. elegans. Genes Dev. 19: 2744–2756. https://doi.org/10.1101/gad.1348205

de Carvalho, C. E., S. Zaaijer, S. Smolikov, Y. Gu, J. M. Schumacher *et al.*, 2008 LAB-1 antagonizes the Aurora B kinase in C. elegans. Genes Dev. 22: 2869–2885. https://doi.org/10.1101/gad.1691208

Dernburg, A. F., K. McDonald, G. Moulder, R. Barstead, M. Dresser *et al.*, 1998 Meiotic recombination in C. elegans initiates by a conserved mechanism and is dispensable for homologous chromosome synapsis. Cell 94: 387–398. https://doi.org/10.1016/S0092-8674(00)81481-6

Derry, W. B., A. P. Putzke, and J. H. Rothman, 2001 Caenorhabditis elegans p53: role in apoptosis, meiosis, and stress resistance Science 294: 591–595. https://doi.org/10.1126/science.1065486

Diag, A., M. Schilling, F. Klironomos, S. Ayoub, and N. Rajewsky, 2018 Spatiotemporal m(i)RNA architecture and 3' UTR regulation in the C. elegans germline. Dev Cell 47: 785–800.e8. https://doi.org/10.1016/j.devcel.2018.10.005

Doerks, T., R. R. Copley, J. Schultz, C. P. Ponting, and P. Bork, 2002 Systematic identification of novel protein domain families associated with nuclear functions. Genome Res. 12: 47–56. https://doi.org/10.1101/gr.203201

Friedland, A. E., Y. B. Tzur, K. M. Esvelt, M. P. Colaiacovo, G. M. Church *et al.*, 2013 Heritable genome editing in C. elegans via a CRISPR-Cas9 system. Nat. Methods 10: 741–743. https://doi.org/10.1038/nmeth.2532

Gabdank, I., and A. Z. Fire, 2014 Gamete-type dependent crossover interference levels in a defined region of Caenorhabditis elegans chromosome V. G3 (Bethesda) 4: 117–120. https://doi.org/10.1534/g3.113.008672

Gartner, A., S. Milstein, S. Ahmed, J. Hodgkin, and M. O. Hengartner, 2000 A conserved checkpoint pathway mediates DNA damage–induced apoptosis and cell cycle arrest in C. elegans. Mol. Cell 5: 435–443. https://doi.org/10.1016/S1097-2765(00)80438-4

Gartner, A., P. R. Boag, and T. K. Blackwell, 2008 Germline survival and apoptosis (September 4, 2008), WormBook, et. The *C. elegans* Research Community, WormBook, doi/10.1895/wormbook.1.145.1, http://www.wormbook.org.

Goodyer, W., S. Kaitna, F. Couteau, J. D. Ward, S. J. Boulton *et al.*, 2008 HTP-3 links DSB formation with homolog pairing and crossing over during C. elegans meiosis. Dev. Cell 14: 263–274. https://doi.org/10.1016/j.devcel.2007.11.016

Govindan, J. A., H. Cheng, J. E. Harris, and D. Greenstein, 2006 Galphao/i and Galphas signaling function in parallel with the MSP/Eph receptor to control meiotic diapause in C. elegans. Curr. Biol. 16: 1257–1268. https://doi.org/10.1016/j.cub.2006.05.020

Govindan, J. A., S. Nadarajan, S. Kim, T. A. Starich, and D. Greenstein, 2009 Somatic cAMP signaling regulates MSP-dependent oocyte growth and meiotic maturation in C. elegans. Development 136: 2211–2221. https://doi.org/10.1242/dev.034595

Gray, S., and P. E. Cohen, 2016 Control of meiotic crossovers: from double-strand break formation to designation. Annu. Rev. Genet. 50: 175–210. https://doi.org/10.1146/annurev-genet-120215-035111

Gumienny, T. L., E. Lambie, E. Hartwieg, H. R. Horvitz, and M. O. Hengartner, 1999 Genetic control of programmed cell death in the Caenorhabditis elegans hermaphrodite germline. Development 126: 1011–1022.

Hajnal, A., and T. Berset, 2002 The C. elegans MAPK phosphatase LIP-1 is required for the G(2)/M meiotic arrest of developing oocytes. EMBO J. 21: 4317–4326. https://doi.org/10.1093/emboj/cdf430

Hans, F., and S. Dimitrov, 2001 Histone H3 phosphorylation and cell division. Oncogene 20: 3021–3027. https://doi.org/10.1038/sj.onc.1204326

Hayashi, M., S. Mlynarczyk-Evans, and A. M. Villeneuve, 2010 The synaptonemal complex shapes the crossover landscape through cooperative assembly, crossover promotion and crossover inhibition during Caenorhabditis elegans meiosis. Genetics 186: 45–58. https://doi.org/10.1534/genetics.110.115501

Hendzel, M. J., Y. Wei, M. A. Mancini, A. Van Hooser, T. Ranalli *et al.*, 1997 Mitosis-specific phosphorylation of histone H3 initiates primarily within pericentromeric heterochromatin during G2 and spreads in an ordered fashion coincident with mitotic

chromosome condensation. Chromosoma 106: 348–360. https://doi.org/10.1007/s004120050256

Hillers, K. J., V. Jantsch, E. Martinez-Perez, and J. L. Yanowitz, 2017 Meiosis (May 4, 2017), *WormBook*, ed. The *C. elegans* Research Community, WormBook, doi/10.1895/wormbook.1.178.1, http://www.wormbook.org. https://doi.org/10.1895/wormbook.1.178.1

Hofmann, E. R., S. Milstein, S. J. Boulton, M. Ye, J. J. Hofmann *et al.*, 2002 Caenorhabditis elegans HUS-1 is a DNA damage checkpoint protein required for genome stability and EGL-1-mediated apoptosis. Curr. Biol. 12: 1908–1918. https://doi.org/10.1016/S0960-9822(02)01262-9

Jantsch, V., P. Pasierbek, M. M. Mueller, D. Schweizer, M. Jantsch *et al.*, 2004 Targeted gene knockout reveals a role in meiotic recombination for ZHP-3, a Zip3-related protein in Caenorhabditis elegans. Mol. Cell. Biol. 24: 7998–8006. https://doi.org/10.1128/MCB.24.18.7998-8006.2004

Jasin, M., and R. Rothstein, 2013 Repair of strand breaks by homologous recombination. Cold Spring Harb. Perspect. Biol. 5: a012740. https://doi.org/10.1101/cshperspect.a012740

Keeney, S., C. N. Giroux, and N. Kleckner, 1997 Meiosis-specific DNA double-strand breaks are catalyzed by Spo11, a member of a widely conserved protein family. Cell 88: 375–384. https://doi.org/10.1016/S0092-8674(00)81876-0

Kelly, K. O., A. F. Dernburg, G. M. Stanfield, and A. M. Villeneuve, 2000 Caenorhabditis elegans msh-5 is required for both normal and radiation-induced meiotic crossing over but not for completion of meiosis. Genetics 156: 617–630.

Kimble, J. E., and J. G. White, 1981 On the control of germ cell development in Caenorhabditis elegans. Dev. Biol. 81: 208–219. https://doi.org/10.1016/0012-1606(81)90284-0

Kosinski, M., K. McDonald, J. Schwartz, I. Yamamoto, and D. Greenstein, 2005 C. elegans sperm bud vesicles to deliver a meiotic maturation signal to distant oocytes. Development 132: 3357–3369. https://doi.org/10.1242/dev.01916

Leacock, S. W., and V. Reinke, 2006 Expression profiling of MAP kinase-mediated meiotic progression in Caenorhabditis elegans. PLoS Genet. 2: e174. https://doi.org/10.1371/journal.pgen.0020174

Lee, M. H., B. Hook, L. B. Lamont, M. Wickens, and J. Kimble, 2006 LIP-1 phosphatase controls the extent of germline proliferation in Caenorhabditis elegans. EMBO J. 25: 88–96. https://doi.org/10.1038/sj.emboj.7600901

Lee, M. H., B. Hook, G. Pan, A. M. Kershner, C. Merritt *et al.*, 2007a Conserved regulation of MAP kinase expression by PUF RNA-binding proteins. PLoS Genet. 3: e233. https://doi.org/10.1371/journal.pgen.0030233

Lee, M. H., M. Ohmachi, S. Arur, S. Nayak, R. Francis *et al.*, 2007b Multiple functions and dynamic activation of MPK-1 extracellular signal-regulated kinase signaling in Caenorhabditis elegans germline development. Genetics 177: 2039–2062. https://doi.org/10.1534/genetics.107.081356

Lettre, G., E. A. Kritikou, M. Jaeggi, A. Calixto, A. G. Fraser *et al.*, 2004 Genome-wide RNAi identifies p53-dependent and -independent regulators of germ cell apoptosis in C. elegans. Cell Death Differ. 11: 1198–1203. https://doi.org/10.1038/sj.cdd.4401488

Libuda, D. E., S. Uzawa, B. J. Meyer, and A. M. Villeneuve, 2013 Meiotic chromosome structures constrain and respond to designation of crossover sites. Nature 502: 703–706. https://doi.org/10.1038/nature12577

Lim, J. G., R. R. Stine, and J. L. Yanowitz, 2008 Domain-specific regulation of recombination in Caenorhabditis elegans in response to temperature, age and sex. Genetics 180: 715–726. https://doi.org/10.1534/genetics.108.090142

Lin, B., and V. Reinke, 2008 The candidate MAP kinase phosphorylation substrate DPL-1 (DP) promotes expression of the MAP kinase phosphatase LIP-1 in C. elegans germ cells. Dev. Biol. 316: 50–61. https://doi.org/10.1016/j.ydbio.2007.12.042

Lui, D. Y., and M. P. Colaiacovo, 2013 Meiotic development in Caenorhabditis elegans. Adv. Exp. Med. Biol. 757: 133–170. https://doi.org/10.1007/978-1-4614-4015-4_6

MacQueen, A. J., M. P. Colaiacovo, K. McDonald, and A. M. Villeneuve, 2002 Synapsis-dependent and -independent mechanisms stabilize homolog pairing during meiotic prophase in C. elegans. Genes Dev. 16: 2428–2442. https://doi.org/10.1101/gad.1011602

Martinez-Perez, E., and A. M. Villeneuve, 2005 HTP-1-dependent constraints coordinate homolog pairing and synapsis and promote chiasma formation during C. elegans meiosis. Genes Dev. 19: 2727–2743. https://doi.org/10.1101/gad.1338505

Martinez-Perez, E., M. Schvarzstein, C. Barroso, J. Lightfoot, A. F. Dernburg *et al.*, 2008 Crossovers trigger a remodeling of meiotic chromosome axis composition that is linked to two-step loss of sister chromatid cohesion. Genes Dev. 22: 2886–2901. https://doi.org/10.1101/gad.1694108

McClendon, T. B., M. R. Sullivan, K. A. Bernstein, and J. L. Yanowitz, 2016 Promotion of homologous recombination by SWS-1 in complex with RAD-51 paralogs in Caenorhabditis elegans. Genetics 203: 133–145. https://doi.org/10.1534/genetics.115.185827

Meneely, P. M., A. F. Farago, and T. M. Kauffman, 2002 Crossover distribution and high interference for both the X chromosome and an autosome during oogenesis and spermatogenesis in Caenorhabditis elegans. Genetics 162: 1169–1177.

Mézard, C., M. T. Jahns, and M. Grelon, 2015 Where to cross? New insights into the location of meiotic crossovers. Trends Genet. 31: 393–401. https://doi.org/10.1016/j.tig.2015.03.008

Miller, M. A., V. Q. Nguyen, M. H. Lee, M. Kosinski, T. Schedl *et al.*, 2001 A sperm cytoskeletal protein that signals oocyte meiotic maturation and ovulation. Science 291: 2144–2147. https://doi.org/10.1126/science.1057586

Mpoke, S. S., and J. Wolfe, 1997 Differential staining of apoptotic nuclei in living cells: application to macronuclear elimination in Tetrahymena. J. Histochem. Cytochem. 45: 675–683. https://doi.org/10.1177/002215549704500505

Murray, J. I., T. J. Boyle, E. Preston, D. Vafeados, B. Mericle *et al.*, 2012 Multidimensional regulation of gene expression in the C. elegans embryo. Genome Res. 22: 1282–1294. https://doi.org/10.1101/gr.131920.111

Nabeshima, K., A. M. Villeneuve, and K. J. Hillers, 2004 Chromosome-wide regulation of meiotic crossover formation in Caenorhabditis elegans requires properly assembled chromosome axes. Genetics 168: 1275–1292. https://doi.org/10.1534/genetics.104.030700

Nabeshima, K., A. M. Villeneuve, and M. P. Colaiacovo, 2005 Crossing over is coupled to late meiotic prophase bivalent differentiation through asymmetric disassembly of the SC. J. Cell Biol. 168: 683–689. https://doi.org/10.1083/jcb.200410144

Nabti, I., P. Marangos, J. Bormann, N. R. Kudo, and J. Carroll, 2014 Dual-mode regulation of the APC/C by CDK1 and MAPK controls meiosis I progression and fidelity. J. Cell Biol. 204: 891–900. https://doi.org/10.1083/jcb.201305049

Nadarajan, S., F. Mohideen, Y. B. Tzur, N. Ferrandiz, O. Crawley *et al.*, 2016 The MAP kinase pathway coordinates crossover designation with disassembly of synaptonemal complex proteins during meiosis. Elife 5: e12039. https://doi.org/10.7554/eLife.12039

Narbonne, P., P. S. Maddox, and J. C. Labbé, 2017 DAF-18/PTEN signals through AAK-1/AMPK to inhibit MPK-1/MAPK in feedback control of germline stem cell proliferation. PLoS Genet. 13: e1006738. https://doi.org/10.1371/journal.pgen.1006738

Ortiz, M. A., D. Noble, E. P. Sorokin, and J. Kimble, 2014 A new dataset of spermatogenic *vs.* oogenic transcriptomes in the

nematode Caenorhabditis elegans. G3 (Bethesda) 4: 1765–1772. https://doi.org/10.1534/g3.114.012351

Paix, A., A. Folkmann, D. Rasoloson, and G. Seydoux, 2015 High efficiency, homology-directed genome editing in Caenorhabditis elegans using CRISPR-Cas9 ribonucleoprotein complexes. Genetics 201: 47–54. https://doi.org/10.1534/genetics.115.179382

Pazdernik, N., and T. Schedl, 2013 Introduction to germ cell development in Caenorhabditis elegans. Adv. Exp. Med. Biol. 757: 1–16. https://doi.org/10.1007/978-1-4614-4015-4_1

Prasad, A., D. F. Porter, P. L. Kroll-Conner, I. Mohanty, A. R. Ryan *et al.*, 2016 The PUF binding landscape in metazoan germ cells. RNA 22: 1026–1043. https://doi.org/10.1261/rna.055871.116

Quevedo, C., D. R. Kaplan, and W. B. Derry, 2007 AKT-1 regulates DNA-damage-induced germline apoptosis in C. elegans. Curr. Biol. 17: 286–292. https://doi.org/10.1016/j.cub.2006.12.038

Reinke, V., H. E. Smith, J. Nance, J. Wang, C. Van Doren *et al.*, 2000 A global profile of germline gene expression in C. elegans. Mol. Cell 6: 605–616. https://doi.org/10.1016/S1097-2765(00)00059-9

Rinaldo, C., P. Bazzicalupo, S. Ederle, M. Hilliard, and A. La Volpe, 2002 Roles for Caenorhabditis elegans rad-51 in meiosis and in resistance to ionizing radiation during development. Genetics 160: 471–479.

Rutkowski, R., R. Dickinson, G. Stewart, A. Craig, M. Schimpl *et al.*, 2011 Regulation of Caenorhabditis elegans p53/CEP-1-dependent germ cell apoptosis by Ras/MAPK signaling. PLoS Genet. 7: e1002238. https://doi.org/10.1371/journal.pgen.1002238

Saito, T. T., J. L. Youds, S. J. Boulton, and M. P. Colaiacovo, 2009 Caenorhabditis elegans HIM-18/SLX-4 interacts with SLX-1 and XPF-1 and maintains genomic integrity in the germline by processing recombination intermediates. PLoS Genet. 5: e1000735. https://doi.org/10.1371/journal.pgen.1000735

Schild-Prüfert, K., T. T. Saito, S. Smolikov, Y. Gu, M. Hincapie *et al.*, 2011 Organization of the synaptonemal complex during meiosis in Caenorhabditis elegans. Genetics 189: 411–421. https://doi.org/10.1534/genetics.111.132431

Schouest, K. R., Y. Kurasawa, T. Furuta, N. Hisamoto, K. Matsumoto *et al.*, 2009 The germinal center kinase GCK-1 is a negative regulator of MAP kinase activation and apoptosis in the C. elegans germline. PLoS One 4: e7450. https://doi.org/10.1371/journal.pone.0007450

Schumacher, B., K. Hofmann, S. Boulton, and A. Gartner, 2001 The C. elegans homolog of the p53 tumor suppressor is required for DNA damage-induced apoptosis. Curr. Biol. 11: 1722–1727. https://doi.org/10.1016/S0960-9822(01)00534-6

Schvarzstein, M., S. M. Wignall, and A. M. Villeneuve, 2010 Coordinating cohesion, co-orientation, and congression during meiosis: lessons from holocentric chromosomes. Genes Dev. 24: 219–228. https://doi.org/10.1101/gad.1863610

Severson, A. F., and B. J. Meyer, 2014 Divergent kleisin subunits of cohesin specify mechanisms to tether and release meiotic chromosomes. Elife 3: e03467. https://doi.org/10.7554/eLife.03467

Severson, A. F., L. Ling, V. van Zuylen, and B. J. Meyer, 2009 The axial element protein HTP-3 promotes cohesin loading and meiotic axis assembly in C. elegans to implement the meiotic program of chromosome segregation. Genes Dev. 23: 1763–1778. https://doi.org/10.1101/gad.1808809

Sukegawa, Y., A. Yamashita, and M. Yamamoto, 2011 The fission yeast stress-responsive MAPK pathway promotes meiosis via the phosphorylation of Pol II CTD in response to environmental and feedback cues. PLoS Genet. 7: e1002387. https://doi.org/10.1371/journal.pgen.1002387

Sulston, J. E., and H. R. Horvitz, 1977 Post-embryonic cell lineages of the nematode, Caenorhabditis elegans. Dev. Biol. 56: 110–156. https://doi.org/10.1016/0012-1606(77)90158-0

Tzur, Y. B., C. Egydio de Carvalho, S. Nadarajan, I. Van Bostelen, Y. Gu *et al.*, 2012 LAB-1 targets PP1 and restricts aurora B kinase upon entrance into meiosis to promote sister chromatid cohesion. PLoS Biol. 10: e1001378. https://doi.org/10.1371/journal.pbio.1001378

Tzur, Y. B., A. E. Friedland, S. Nadarajan, G. M. Church, J. A. Calarco *et al.*, 2013 Heritable custom genomic modifications in Caenorhabditis elegans via a CRISPR-cas9 system. Genetics 195: 1181–1185. https://doi.org/10.1534/genetics.113.156075

Tzur, Y. B., E. Winter, J. Gao, T. Hashimshony, I. Yanai *et al.*, 2018 Spatiotemporal gene expression analysis of the Caenorhabditis elegans germline uncovers a syncytial expression switch. Genetics 210: 587–605. https://doi.org/10.1534/genetics.118.301315

Weiner, M. P., G. L. Costa, W. Schoettlin, J. Cline, E. Mathur *et al.*, 1994 Site-directed mutagenesis of double-stranded DNA by the polymerase chain reaction. Gene 151: 119–123. https://doi.org/10.1016/0378-1119(94)90641-6

Woglar, A., A. Daryabeigi, A. Adamo, C. Habacher, T. Machacek *et al.*, 2013 Matefin/SUN-1 phosphorylation is part of a surveillance mechanism to coordinate chromosome synapsis and recombination with meiotic progression and chromosome movement. PLoS Genet. 9: e1003335. https://doi.org/10.1371/journal.pgen.1003335

Ye, A. L., J. M. Ragle, B. Conradt, and N. Bhalla, 2014 Differential regulation of germline apoptosis in response to meiotic checkpoint activation. Genetics 198: 995–1000. https://doi.org/10.1534/genetics.114.170241

Yin, Y., S. Donlevy, and S. Smolikove, 2016 Coordination of recombination with meiotic progression in the Caenorhabditis elegans germline by KIN-18, a TAO kinase that regulates the timing of MPK-1 signaling. Genetics 202: 45–59. https://doi.org/10.1534/genetics.115.177295

Yokoo, R., K. A. Zawadzki, K. Nabeshima, M. Drake, S. Arur *et al.*, 2012 COSA-1 reveals robust homeostasis and separable licensing and reinforcement steps governing meiotic crossovers. Cell 149: 75–87. https://doi.org/10.1016/j.cell.2012.01.052

Youds, J. L., D. G. Mets, M. J. McIlwraith, J. S. Martin, J. D. Ward *et al.*, 2010 RTEL-1 enforces meiotic crossover interference and homeostasis. Science 327: 1254–1258. https://doi.org/10.1126/science.1183112

Zetka, M., 2009 Homologue pairing, recombination and segregation in Caenorhabditis elegans. Genome Dyn. 5: 43–55. https://doi.org/10.1159/000166618

Zhang, L., Y. Liang, Y. Liu, and C. L. Xiong, 2010 The role of brain-derived neurotrophic factor in mouse oocyte maturation in vitro involves activation of protein kinase B. Theriogenology 73: 1096–1103. https://doi.org/10.1016/j.theriogenology.2010.01.009

Communicating editor: M. Sundaram